~~An improved~~ A new conceptual model ~~of Quaternary global ice volume and~~ reveals a long ramp-like change as cause for the Mid-Pleistocene Transition

Felix Pollak[1,2,5], Frédéric Parrenin[1], Émilie Capron[1], Zanna Chase[2,3], Lenneke Jong[4,5], and Etienne Legrain[6,7]

[1]Université Grenoble Alpes, CNRS, INRAE, IRD, Grenoble INP, IGE, Grenoble, France
[2]Institute for Marine and Antarctic Studies, University of Tasmania, Hobart, TAS, Australia
[3]Australian Research Council Centre for Excellence in Antarctic Science (ACEAS), University of Tasmania, Hobart, TAS, Australia
[4]Australian Antarctic Division, Department of Climate Change, Energy, the Environment and Water, Kingston, TAS, Australia
[5]Australian Antarctic Program Partnership, Institute for Marine and Antarctic Studies, University of Tasmania, Hobart, TAS, Australia
[6]Laboratoire de Glaciologie, Université libre de Bruxelles, Brussels, Belgium
[7]Department of Water and Climate, Vrije Universiteit Brussel, Brussels, Belgium

Correspondence: Felix Pollak (felix.pollak@univ-grenoble-alpes.fr)

Abstract. During the Quaternary period, spanning the last 2.6 million years, the characteristic frequency and amplitude of glacial-interglacial cycles evolved from low-amplitude 41,000-year cycles to high-amplitude 100,000-year cycles. This transition occurred around 1.2 to 0.8 million years ago and is referred to as the Mid-Pleistocene Transition (MPT). ~~While the 41 kyr cycles are driven by changes in Earth's obliquity, which largely affect the incoming solar insolation, no apparent change in~~ The absence of any significant change in the external orbital forcing during this period ~~could explain the shift towards 100 kyr cycles. Several theories have been put forward to explain this shift, including scenarios of both gradual and abrupt changes in the internal climate systemthroughout the Pleistocene. In order to test which theory best matches the observations, we have constructed a conceptual model capable of simulating changes in the global ice volume over the past 2.6 Ma and accurately reconstructing the MPT and its associated change in amplitude and frequency. Four different forcing scenarios are implemented, ranging from a purely orbitally driven model to~~ suggests the existence of some fundamental change within the Earth-climate system, leading to non-linearities or feedback mechanisms. The temporal structure of such a change is still under debate. Here, we present a new conceptual model of the Quaternary global climate, the so-called RAMP model. It can be applied to different paleoclimatic records and variables as the global mean sea level, benthic foraminifera $\delta^{18}O$ and seawater $\delta^{18}O_{sw}$. The RAMP model incorporates a ramp-like change in ~~internal forcing. The model is in favour of a ramp-like forcing scenario, where the gradual change in internal forcing is limited in time and started around 2 Ma~~its deglaciation threshold to reconstruct the MPT. Parameter optimization finds that the onset of the change occurs in the early Quaternary (2.6 - 2.2 Ma) and lasts into the 100 kyr world (500 - 250 ka). These findings ~~imply that the climate system had already undergone major changes in the early Pleistocene and~~ support the idea of a long-term ~~climatic~~ shift as a cause of the MPT ~~. For the best-performing model , we included an ice volume dependency in the state thresholds, demonstrating that glacial terminations during the past~~

900 ka are mainly driven by precession rather than obliquity. and imply that the climate shift began early in the Quaternary. The model uses a linear combination of precession and obliquity as external orbital forcing, which can be optimized to best reconstruct the target paleoclimatic record. The identified orbital forcing differs from the widely used insolation at summer solstice at 65° N, as it exhibits a larger precession signal. While the RAMP model yields consistent and good results for two global mean sea level curves and one benthic δ^{18}O record, it fails in reconstructing a recent deconvolution into seawater $\delta^{18}O_{sw}$, which significantly differs from the other curves. Moreover, we perform various sensitivity tests, in which the RAMP model demonstrates high robustness, especially the identified long-term trend is a very robust feature in the model, indicating its importance in reconstructing the MPT.

1

The Quaternary is the most recent geological epoch, covering the last 2.6 Ma. It is characterized by the alternance of cold glacial climate states and warmer interglacial periods. Glaciers and ice sheets expanded during glacial periods and retreated during interglacial periods. In the first half of the 20th century, Milutin Milankovitch made significant contributions to the astronomical theory of climate, which links changes in Earth's orbital parameters to changes in the radiative forcing, which ultimately leads to glacial-interglacial variability (Milankovitch, 1941). In his theory, the orbital variations of Earth's eccentricity, obliquity and precession lead to variations in the insolation during boreal summer, which is the dominating driver of glacial cycles (Ganopolski, 2024). Earth's obliquity varies on a cycle of approximately 41 kyr, while precession operates over a 19 kyr and a 23 kyr period, and eccentricity fluctuates on a 100 kyr and a 400 kyr timescale (Hays et al., 1976). In his theory, the orbital variations of Earth's eccentricity, obliquity and precession lead to variations in the insolation during boreal summer, which is the dominating driver of glacial cycles (Ganopolski, 2024).

Two central problems arise from this theory: . The first is known as the 100 kyr problem. : The late Quaternary glacial cycles (approximately the last 800 ka) were characterized by follow 100 kyr cycles, closely following the eccentricity signal. They show a "sawtooth" pattern of long, roughly 90 kyr long glaciations, followed by short, roughly 10 kyr long deglaciations (Raymo and Huybers, 2008). However, changes in insolation are mainly dominated by the obliquity and precession signal, while the influence of eccentricity on the annual averaged global insolation is negligible (Imbrie et al., 2011; Barker et al., 2022) . So why is there a 100 kyr signal in the glacial cyclicity? This underlines the more complex interplay between eccentricity and climate and the possible existence of feedback mechanisms or other non-linearities, which are needed to explain this influence (Paillard, 2015; Imbrie et al., 2011).

patterns, despite the eccentricity having only a negligible influence on the global insolation compared to the obliquity and precession (Raymo and Huybers, 2008; Imbrie et al., 2011; Barker et al., 2022). The second issue is related to the shift of low-amplitude roughly ~ 41 kyr cycles towards high-amplitude roughly ~ 100 kyr cycles during the mid-Pleistocene (~1.2 - 0.8 Ma) in the absence of any significant change in orbital forcing. This transition is known as the Mid-Pleistocene Transition (MPT) (Imbrie et al., 2011; Barker and Knorr, 2023; Elderfield et al., 2012). The occurrence of the MPT poses one of the most challenging open questions to the paleoclimatological community and has been the subject of intense studies (Willeit et al.,

2019; Legrain et al., 2023; Berends et al., 2021b; Ganopolski, 2024). ~~Due to the lack of any apparent change in orbital forcing, various~~ Various internal feedback mechanisms of the climate system and non-linearities have been put forward to explain this major climatic shift (Legrain et al., 2023; Berends et al., 2021b).

~~Clark and Pollard (1998) proposed the so-called regolith hypothesis as a potential cause of the MPT. Before the onset of the Northern Hemisphere glaciations, 2.6 Ma, the North American and Eurasian surface was covered by a thick layer of regolith (10-50 m), which was formed due to exposure to weathering over the last 10^7 – 10^8 years. The lower friction and deformability of the regolith increased the basal flow velocity, leading to thinner and wider ice sheets, which spread further south during the early Pleistocene. Hence, the enlarged ablation zones became more sensitive to insolation~~Recent studies suggest that the duration and timing of deglaciation and glaciation events over the last 900 ka were largely deterministic and driven by the relative phasing of precession, obliquity, and eccentricity (Barker et al., 2022, 2025). Barker et al. (2025) identified candidate precession peaks, which are precession peaks that begin while obliquity is increasing, as essential for glacial terminations. They found that all glacial terminations during the last 900 ka correspond to the first candidate precession peak after a minimum in eccentricity. This is how the 100 kyr periodicity comes into play for the post-MPT world. On the other hand, it seems like obliquity alone controls the following glacial inception, which is triggered by the start of its next decreasing phase. During and prior to the MPT, the authors found that almost all candidate precession peaks are linked to glacial terminations. Since they depend on rising obliquity values, they are mainly paced by obliquity, resulting in the observed ~~obliquity-driven~~ 41 kyr world ~~. The continuous glaciations gradually removed the regolith beneath, exposing the unweathered~~ with no more influence of eccentricity on these cycles. This leaves open the question of why there was a change in the climate response to candidate precession peaks.

While various hypotheses have been proposed to explain the MPT, the following two are particularly popular. The regolith hypothesis suggests that gradual removal of thick regolith layers (10-50 m) on the North American and Eurasian surface during continuous glaciations exposed the high-friction crystalline bedrock ~~, corresponding to reduced basal velocities and a reduced sensitivity to insolation. The increased~~ underneath, reducing basal ice flow and increasing ice sheet stability~~would have resulted in the observed late-Pleistocene ~~~~, leading to the observed 100 kyr ~~glacial-interglacial periodicity (Clark et al., 2006; Berends et al., 2021b; ~~

~~Another commonly proposed hypothesis to explain the MPT concerns~~ periodicity (Clark and Pollard, 1998; Clark et al., 2006; Willeit et . Alternatively, a gradual cooling trend~~due to a continuous long-term decrease of~~ , associated with a decrease in atmospheric CO_2 concentrations throughout the Quaternary~~(Berends et al., 2021b; Willeit et al., 2019; ?)~~, may have triggered the MPT (Scherrenberg et al., 2025). Based on such a long-term cooling trend, various feedback mechanisms ~~, like ice sheet feedback mechanisms~~ in the ice sheet or changes in the ocean circulations ~~,~~ have been proposed as a secondary trigger for the MPT (Berends et al., 2021b).

Another open question ~~is whether an abrupt or gradual scenario~~ concerns the temporal structure of the change that might have triggered the MPT. While a gradual ~~change~~ scenario involves a linear change ~~of a climatic parameter~~ over the entire Quaternary ~~, an abrupt scenario refers to~~ (like the CO_2 hypothesis), a more abrupt scenario involves the crossing of ~~a climatic threshold, which leads to a new, irreversible climate state. A scenario leading to such an abrupt transition is considered to have~~

lasted only a limited time and not over the entire Quaternary (Legrain et al., 2023). While the CO_2 hypothesis is an example of a gradual theory, one some irreversible climatic thresholds over a short period of time (Legrain et al., 2023). One proposed abrupt mechanism that could have contributed to the MPT is based on involves non-linear feedback effects between the ice sheets and the global climate. In particular, it has been proposed that from the merging of the North American Laurentide and Cordilleran ice sheets posed a strong feedback on the glacial cycles (Berends et al., 2021b; Bintanja and van de Wal, 2008; Gregoire et al., 2012). A long-term cooling trend is suggested to have allowed the North American ice sheets to cross the threshold of around 45 m sl (meter sea level equivalent), needed to merge the Laurentide and Cordilleran ice sheets for the first time around 1 Ma (Bintanja and van de Wal, 2008; Berends et al., 2021b). While their merging would have led to further ice volume increase without any change in the solar forcing (Berends et al., 2021b), the increased ice volume would exhibit instabilities once exceeding ~70 m sl, leading to rapid deglaciations triggered by the next insolation peak, resulting in the observed 100 kyr cycles of the post-MPT world (Bintanja and van de Wal, 2008; Gregoire et al., 2012).

Climate models of varying complexity present a versatile tool for investigating these different hypotheses. On one end of the model hierarchy are They range from computationally expensive Earth System Models that try to include the underlying physics and couple different compartments of the climate system, for example, the cryosphere with the carbon cycle to account for different feedback mechanisms. Their more realistic representation of the climate system comes at the cost of high computational demand. This is a particular obstacle for the long simulation periods that are required ($\mathcal{O}$(Myr)), as well as for running large ensembles of simulations, needed for parameter tuning, sensitivity experiments, or investigation of various parameterizations. On the other end of the model hierarchy are so-called conceptual models that are to simple, zero-dimensional (spatial dimensions) representations of the climate system. The basic idea of these types of models is to reduce the model complexity by focusing conceptual models that focus on key variables while allowing long simulations. They rely on a reduced number of highly aggregated macroscopic variables that try to reconstruct the full dynamics as closely as possible (Saltzman, 2001). Verbitsky and Crucifix (2023) point out that a mathematical model must be simple enough to physically interpret the simulation results. Due to the reduced number of model parameters, it becomes easier to interpret the influence of individual parameters or parameterizations on the simulation outcomes through their straightforward removal or inclusion. Furthermore, their reduced number of parameters makes the necessary tuning process more manageable and allows for long simulation periods ($\mathcal{O}$(Myr)). Hence, conceptual models serve as a crucial tool to investigate the MPT and glacial-interglacial variability across the Quaternary.

Various conceptual models have been developed over the last decades, varying in their underlying assumptions and hypotheses. Many of them yield good results and can reconstruct the 100 kyr world with its characteristic saw-tooth pattern (Gildor and Tziperman, 2001; Imbrie et al., 2011; Parrenin and Paillard, 2012; Pérez-Montero et al., 2024) or even the MPT with its shift in amplitude and frequency and its specific timing (Paillard, 1998; Paillard and Parrenin, 2004; Legrain et al., 2023; Ganopolski, 2024).

A common approach is to attribute glacial-interglacial variability to relaxation oscillations between multiple equilibria (Paillard, 1998; Parrenin and Paillard, 2012; Legrain et al., 2023; Leloup and Paillard, 2022). In his initial work, Paillard (1998) proposed a three-state model (hereafter referred to as P98) consisting of an interglacial, mild glacial, and a full glacial

state. Transitions between model states depend on the ice volume and the insolation. To account for a change in forcing due to decreasing atmospheric CO_2 concentrations, he added a small linear trend in the radiative forcing and linearly increased one of the state thresholds. This model is able to accurately reconstruct the global ice volume over the past 2 Ma, with good results in the timing of terminations and the change in periodicity due to the MPT. In later work, Parrenin and Paillard (2012) presented an improved version of this model ~~, which now~~ (hereafter referred to as PP12), which only consists of a glaciation and a deglaciation state. While the deglaciation trigger depends on a combination of ice volume and insolation, the glacial inception is solely controlled by insolation. Moreover, they adapted the solar forcing, such that the model takes a linear combination of three orbital parameters instead of a fixed insolation curve. A similar approach was used in the model of Imbrie et al. (2011). Indeed, the model results seem to depend on the chosen insolation forcing, since they differ in their contributions from obliquity and precession (Leloup and Paillard, 2022). ~~Legrain et al. (2023)~~ The three model versions by Legrain et al. (2023) (hereafter referred to as L23 models) continued the work by implementing different internal forcing scenarios to test which of them is most likely to reproduce the MPT. In addition to the external solar forcing, they added ~~an internal forcing~~ internal variations to the model in the form of a varying deglaciation threshold. They found that a gradual increase of this deglaciation threshold is more likely to reproduce the MPT than an abrupt change. Based on this finding, they suggested that a gradual decline in atmospheric CO_2 concentrations over the Pleistocene may have increased the deglaciation threshold, potentially causing the MPT.

~~Gildor and Tziperman (2001) used an idealized model to study the influence of different sea ice feedback mechanisms to explain the 100 kyr cycles. They suggested that the large extent of sea ice during late glacial periods would have reduced atmospheric temperatures, humidity, and evaporation. Thus, the available precipitation would have decreased, leading to negative mass balances and quick terminations. Their model links the 100 kyr cycles fully to this sea ice switch, in the absence of any external forcing. However, their model fails to reproduce some key climatic features because of its high idealization, hence missing feedback mechanisms other than those related to sea ice changes.~~

Imbrie et al. (2011) proposed a phase-space model that again combines ice volume and orbital forcing as a deglaciation trigger. They were able to reproduce the shift in frequency of glacial-interglacial cycles purely by orbital forcing, without changing any model parameters during the MPT. Hence, they linked the occurrence of 100 kyr glacial cycles to the eccentricity-driven amplitude modulation of precession. However, their model-data comparison was limited to a detrended benthic $\delta^{18}O$ curve rather than an ice volume reconstruction, thereby precluding the assessment of whether their model accurately reconstructs the change in amplitude over the MPT.

In a more recent work, Ganopolski (2024) attempted to set up a generalized Milankovitch Theory by incorporating model results from CLIMBER-2 (a more sophisticated Earth-System Model) into a conceptual model. The model can reproduce the glacial cycles of the Quaternary based on the nonlinear response of the climate system to the orbital forcing in the form of the eccentricity-driven amplitude modulation of precession and the existence of supercritical ice sheets. A gradual increase ~~of~~ in the critical ice volume is added to model the MPT. The author associates this with the gradual removal of terrestrial sediments in the Northern Hemisphere, which is needed to prolong the late-Pleistocene glacials.

Due to their higher complexity, it is more difficult to identify the main mechanisms driving the glacial-interglacial variability for more comprehensive climate models, which explicitly resolve various physical processes to improve the model accuracy. In contrast, the strength of conceptual models is their simple conceptual framework, which allows for straightforward isolation of the key mechanisms, but therefore, they often lack a profound physical basis or depend on mathematical thresholds. In recent work, Pérez-Montero et al. (2024) presented a more sophisticated conceptual model to bridge these two approaches. Their model aims to simulate the interactions between the climate and the Northern Hemisphere ice sheets, despite a reduced spatial dimensionality in the fundamental equations. They obtain good results for various paleoclimatic records. However, they only focused on the last 800 ka.

Some of the above-mentioned conceptual models are limited by short simulation periods, which do not cover the MPT (Parrenin and Paillard, 2003; Pérez-Montero et al., 2024) or they rely on a single insolation metric for the orbital forcing (Ganopolski, 2024 . In this study, we use the well-suited conceptual modelling approach to investigate the climatic variations of the Quaternary. Our objective is to develop a versatile conceptual model that can be easily applied to different forcing scenarios and can be run on different simulation periods, covering the entire MPT. Moreover, we reduce model biases by not relying on a single insolation metric, but rather use a linear combination of different orbital parametersimprove the 2-state L23 conceptual models. To account for potential feedback mechanisms in the climate system , we implement various internal forcing scenarios in the model, ranging from a purely orbital model to a or internal changes in the system, we implement a new ramp-like change in internal forcingscenario, called the RAMP model. Here, the focus is lies on the general temporal structure of such a potential feedback mechanism, which allows change, allowing for its physical interpretation. Our model is a continuation of the 2-state Legrain (2023) model and simulates the change in global ice volume.The modular design of our model facilitates easy adaptation to a wide range of research questions. We demonstrate this flexibility by modifying the model to investigate the sensitivity of large ice sheets to changes in orbital parameters during the late Pleistocene. Furthermore, we extrapolate the model to project glacial-interglacial variability over the next 250 kyrThe RAMP model covers all three temporal scenarios discussed in the L23 models and is characterized by its easy adjustability. In comparison with the L23 models, it can be run on different time scales, be extrapolated into the future, be run on different tuning targets and for different climatic variables (global mean sea level, $\delta^{18}O$), and it can be easily re-tuned for new parameterizations (e.g. allowing to test the effects of changes in the state thresholds, forcing, etc.).

2 Methods

2.1 Base modelsThe RAMP modelused in this study is

The new RAMP model presents an improved version of the conceptual model developed by Legrain et al. (2023), which is based on the work by Parrenin and Paillard (2012). The model is externally forced by obliquity and precession L23 models. In the following, the model formulation is described. A detailed description of the changes compared to the L23 models can be found in the Supplementary Information (SI Sec. 1).

While the L23 models were used to simulate the global ice volume ~~$v(t)$ in meter sea-level equivalent (m sl) over the Pleistocene. As input, it uses~~ and relied on the sea level reconstruction by Berends et al. (2021a) as a tuning target, the RAMP model can be applied to various targets, including benthic foraminifera and seawater δ^{18}O. Targets, other than global ice volume, are scaled to the Berends et al. (2021a) sea level, then solved for this unit space, before being rescaled to their initial units. This allows for consistent parameter units for all tuning targets and comparable orders of magnitude, and, therefore, to use a single model for various dimensional paleoclimatic records.

The RAMP model uses orbital forcing as an input to reconstruct a paleoclimatic curve over the Quaternary. Leloup and Paillard (2022) showed that the model outcome depends on the chosen insolation forcing (e.g. summer solstice or caloric season at 65° N). This poses a bias to the model by selecting a specific insolation metric. Some earlier models (Imbrie et al., 2011; Parrenin and Paillard, 2012; Leg use instead a linear combination of ~~three orbital parameters normalized to zero mean and unit variance that can reproduce the~~ precession, co-precession and obliquity, which can represent insolation at most latitudes and seasons ~~(Loutre, 1993; Imbrie et al., 2011)~~ (Imbrie et al., 2011). In the RAMP model, we only use a linear combination of precession and obliquity. We show that such a linear combination of only two orbital parameters can indeed accurately reconstruct various insolation curves (SI Sec. 4). The following orbital parameters (dimensionless) from La2004 orbital solution (Laskar et al., 2004) are used:

$$\text{Esi: Precession} \sim e\sin(\omega), \text{Eco: Phase-shifted precession} \sim e\cos(\omega): \text{Precession parameter} \sim e\sin(\omega), \tag{1}$$

$$\text{Ob: Obliquity} \sim \epsilon, \tag{2}$$

with ω the precession angle taken from the vernal equinox and e the eccentricity.
Hence, the orbital forcing $I(t)$ ($\mathrm{m\,kyr^{-1}}$) in the model is defined as:

$$I(t) = \alpha_{\mathrm{Esi}}\mathrm{Esi}(t) + \alpha_{\mathrm{O}}\mathrm{Ob}(t), \tag{3}$$

with the constant weights α_{Esi} and α_{O} ($\mathrm{m\,kyr^{-1}}$).

The model has two different states, the glaciation state (**g**) and the deglaciation state (**d**). Therefore, the ~~ice volume evolution~~ paleoclimatic quantity $v(t)$, given in meter sea level equivalent (m sl), is driven by two ~~linear~~ first-order differential equations, depending on the current model state:

$$\mathrm{g}: \frac{\mathrm{d}v(t)}{\mathrm{d}t} = -I_{\alpha}(t) + \alpha_{\mathrm{g}} = -I_{\alpha}(t) + \alpha_g, \tag{4}$$

$$\mathrm{d}: \frac{\mathrm{d}v(t)}{\mathrm{d}t} = -I_{\alpha}(t) + \alpha_{\mathrm{d}} - \frac{v(t)}{\tau_{\mathrm{d}}(t)} = -I_{\alpha}(t) + \alpha_{\mathrm{d}} - \frac{v(t)}{\tau_{\mathrm{d}}(t)}\frac{v(t)}{\tau_{\mathrm{d}}}, \tag{5}$$

where ~~α_{Esi}, α_{Eco}, α_{O}, α_{g} and α_{d} are constant model parameters in~~ α_{g} ($\mathrm{m\,kyr^{-1}}$~~. $\tau_{\mathrm{d}}(t)$ is the relaxation time in~~) is a constant model parameter controlling the glacial rate of advance and τ_{d} (kyr) is the constant relaxation time, which controls the deglacial rate of retreat.

A state change from a glaciation to a deglaciation (**g**) $\rightarrow$ (**d**) occurs when a combination of the current ~~ice volume~~ quantity $v(t)$ and the orbital forcing exceeds a critical threshold~~. Hence, a termination can be triggered for moderate orbital values if~~

~~the ice volume is large, or vice versa when the current ice volume is moderate, but the orbital forcing is large:~~

~~(i)~~ $$v(t) + \underbrace{(k_{\mathrm{Esi}}\mathrm{Esi}(t) + k_{\mathrm{Eco}}\mathrm{Eco}(t) + k_{\mathrm{O}}\mathrm{Ob}(t))}_{=I_k(t)} = v(t) + I_k(t) > v_0(t),$$

~~(ii)~~ $$\underbrace{k_{\mathrm{Esi}}\mathrm{Esi}(t) + k_{\mathrm{Eco}}\mathrm{Eco}(t) + k_{\mathrm{O}}\mathrm{Ob}(t)}_{=I_k(t)} = I_k(t) \geq v_1,$$

⋮

(i) $v(t) \cdot \tilde{I}(t) + v(t) > v_0(t)$ & (ii) $v(t) \cdot \tilde{I}(t) > v_1$. (6)

~~where k_{Esi}, k_{Eco} and k_{O} are constant model parameters in . While $v_0(t)$ is the deglaciation parameter in and can vary in time depending on the specific model configuration, v_1 is another model threshold in but constant in time.~~

~~Conversely~~Vice versa, a transition from a deglaciation state to a glaciation state (**d**) → (**g**) occurs when:

~~(i)~~ $$\underbrace{k_{\mathrm{Esi}}\mathrm{Esi}(t) + k_{\mathrm{Eco}}\mathrm{Eco}(t) + k_{\mathrm{O}}\mathrm{Ob}(t)}_{=I_k(t)} = I_k(t) < v_1,$$

~~(ii)~~ $$v(t) + \underbrace{(k_{\mathrm{Esi}}\mathrm{Esi}(t) + k_{\mathrm{Eco}}\mathrm{Eco}(t) + k_{\mathrm{O}}\mathrm{Ob}(t))}_{=I_k(t)} = v(t) + I_k(t) \leq v_0(t).$$

(i) $v(t) \cdot \tilde{I}(t) + v(t) < v_0(t)$ & (ii) $v(t) \cdot \tilde{I}(t) < v_1$. (7)

~~In addition to the external forcing described by the orbital parameters, the model can also incorporate an internal forcing mechanism to account for non-linear feedback mechanisms within the climate system. The model has four different configurations:~~

~~(i) **ORB**: The orbital model is purely orbitally driven and the deglaciation parameter $v_0(t) = v_0$ and the relaxation time $\tau_d(t) = \tau_d$ are~~ To account for the correct units, the threshold equations use the dimensionless orbital forcing $\tilde{I}(t) = \frac{I(t)}{[I]}$. The time-dependent deglaciation parameter is denoted as $v_0(t)$ (m), and v_1 (m) is another model threshold but constant in time. Supplementary Figure S3 visualizes how these thresholds act in the RAMP model and how they initiate state changes and drive the dynamics of the model.

~~(ii) **ABR**: The abrupt model includes an abrupt change at t_{abr} for the deglaciation parameter and the relaxation time:~~

$$v_0(t) = \begin{cases} v_0', & \text{if } t \geq t_{abr} \\ v_0, & \text{if } t < t_{abr} \end{cases} \qquad \tau_d(t) = \begin{cases} \tau_d', & \text{if } t \geq t_{abr} \\ \tau_d, & \text{if } t < t_{abr} \end{cases}$$

~~with v_0' and v_0 being constant values for the deglaciation parameter before and after the abrupt shift. And with τ_d' and τ_d being constant values for the relaxation time before and after the abrupt shift.~~

~~(iii) **GRAD**: The gradual model includes a gradual change of~~ To simulate the MPT, the L23 models (and their earlier precursor models) introduced a temporal change in the deglaciation parameter ~~and the relaxation time over the whole simulation~~

period:

$v_0(t) = v_0 - C_v t$

$\tau_d(t) = \tau_d - C_\tau t$

where v_0 and τ_d are constants and define the values at $t = 0$. C_v and C_τ describe the rate of change () of the deglaciation parameter and the relaxation time, respectively.

(iv) **RAMP**: The ramp-like model includes a ramp-like change of the deglaciation parameter and the relaxation time. Both parameters change $v_0(t)$, as orbital forcing alone was not capable of simulating the MPT in their model. In the RAMP model, this parameter is altered ramp-like, i.e. it changes linearly during a period bounded by t_1 and t_2 . Before and after this period, both parameters are constant :

Time evolution of $v_0(t)$ and $\tau_d(t)$ for the RAMP model.

(ka) and stays constant before and after:

$$v_0(t) = \begin{cases} \tau_d(t) = & v_{0,1}, & \text{if } t > t_1 \\ & v_{0,1} + \frac{v_{0,2} - v_{0,1}}{t_2 - t_1}(t - t_1), & \text{if } t_1 \geq t \geq t_2 \\ & v_{0,2}, & \text{if } t_2 > t \end{cases} \tag{8}$$

with v_0' and τ_d' the constant values with $v_{0,1}$ (m) the constant value before the ramp and with v_0 and τ_d the constant values $v_{0,2}$ (m) the constant value after the ramp. In the case that $t_1 = t_2$, the RAMP model converges towards the ABR model. If t_2 is set to the beginning of the simulation and $t_1 = 0$, the RAMP model converges to the GRAD model , with a linear trend over the whole simulation period . Due to this formulation, the The time t is conventionally given in paleo units (ka BP). This implementation covers three special temporal scenarios, all included in the three model versions discussed in L23:

- if $v_{0,1} = v_{0,2}$: no change in the deglaciation parameter. RAMP is only externally forced by changes in orbital parameters (equivalent to ORB model in L23)
- if $t_1 = t_2$: abrupt jump in $v_0(t)$ (equivalent to ABR model in L23)
- if $t_1 = 2.6$ Ma and $t_2 = 0$ Ma: gradual trend over entire simulation period (equivalent to GRAD model in L23)

Therefore, the new RAMP model is more flexible than any of the L23 models, and for a linear trend in v_0, it also gives information on when such a trend has started and ended. Tuning the RAMP model serves as a bridge between the ABR and the GRAD model and can be used to verify which scenario is more likely. Furthermore, it allows us to investigate the duration and start point of the linear trend. to some paleoclimatic target curve reveals the temporal evolution in $v_0(t)$, needed to best reproduce this curve.

2.2 RAMP-l model

Beyond the standard RAMP model outlined above, we develop a slightly modified version. This version introduces three additional parameters, referred to as the l-parameters, hence it is denoted as the RAMP-l model . Here, the term I_k in In contrast

to the L23 models, the newly developed RAMP model demonstrates superior numerical efficiency, exhibiting a speedup by a factor of approximately 30, and it incorporates a more advanced tuning strategy (more details in SI Sec. 1). The gain in numerical efficiency in combination with a more refined tuning strategy allowed us to test various parameterizations involving modifications to the model forcing, the evolutionary equations, or the threshold equations (~~Eq. 6, 7)which is linked to the orbital forcing is adapted by the unitless parameters l_{Esi}, l_{Eco} and l_{O}:~~

$$\begin{aligned}\tilde{I}_k &= [k_{\mathrm{Esi}} + l_{\mathrm{Esi}} v(t)]\,\mathrm{Esi}(t) + [k_{\mathrm{Eco}} + l_{\mathrm{Eco}} v(t)]\,\mathrm{Eco}(t) + [k_{\mathrm{O}} + l_{\mathrm{O}} v(t)]\,\mathrm{Ob}(t) \\ &= \underbrace{k_{\mathrm{Esi}}\mathrm{Esi}(t) + k_{\mathrm{Eco}}\mathrm{Eco}(t) + k_{\mathrm{O}}\mathrm{Ob}(t)}_{=I_k(t)} + \underbrace{l_{\mathrm{Esi}} v(t)\mathrm{Esi}(t) + l_{\mathrm{Eco}} v(t)\mathrm{Eco}(t) + l_{\mathrm{O}} v(t)\mathrm{Ob}(t)}_{=I_l(t)} \\ &= I_k(t) + I_l(t)\ .\end{aligned}$$

~~This new parameterization adds to the I_k term another term, called I_l, which depends on the ice volume. A larger ice volume leads to a larger I_l term. With the increasing global ice volume during the late Quaternary, this term is becoming more significant than it was in the early Quaternary. The multiplication of the ice volume and the orbital parameters ensures that these three additional terms mainly affect the forcing at time points of large ice volume and extrema in the respective orbital parameter. Therefore, this parameterization implements the sensitivity of large ice volumes to changes in orbital parameters.~~

~~To investigate the influence of the different orbital forcing scenarios, we do not include this model for~~ SI Tab. S4). These tests enabled us to investigate the influence of various parameters and to identify less important ones that could be excluded from the final model. During this process, we identified the necessity of scaling the orbital forcing I in the threshold equation in such a way that it has a similar magnitude to the quantity v. Consequently, this allowed for a reduction in the number of parameters in the ~~comparison of the four standard models (ORB, ABR, GRAD, RAMP), since these models only differ in their internal forcing, which allows isolating this effect on the simulation outcome. We only use the RAMP-l model to identify the influence of the additional l-parameters and to see how this affects the simulated outcomes~~ model compared to the ~~standard RAMP model. Furthermore, we can investigate the role of the three different orbital parameters on large ice volumes and test the hypothesis that large ice volumes become more sensitive to precession in the late Quaternary, and thus, these glacial terminations are mainly determined by precession rather than obliquity (Barker et al., 2025)~~L23 models (by 2 to 4 fewer), while simultaneously covering a broader range of temporal scenarios and improving the performance of the model.

2.2 ~~Global ice volume reconstructions~~Tuning targets

The ~~different model configurations are all fitted to a global sea level reconstruction by Berends et al. (2021a). Since the simulated~~ L23 model reconstructed the global ice volume ~~in the model is expressed in meter sea level equivalent (m sl) , it can be directly compared to sea level curves. An optimal set of parameters is inferred by using a Monte Carlo method which best fits the model to the target sea level data (see next section).~~ over the past 2 Ma by using the global mean sea level (GMSL) reconstruction by Berends et al. (2021a) as a tuning target. In contrast, the RAMP model is extended to include four different paleoclimatic records, which allow reconstructing not only the global ice volume, but also benthic $\delta^{18}O_b$ and seawater $\delta^{18}O_{sw}$.

The Berends sea level data reconstructs the past 3.6 Ma, based on an inverse forward modelling approach that aims to disentangle the coupled signals of ice volume and ocean temperature, present in benthic δ^{18}O records (Berends et al., 2021a). It uses the LR04 stack of benthic δ^{18}O as ~~a forcing (Lisiecki and Raymo, 2005)and has a high temporal resolution of 100 years.~~

~~To avoid relying on a single data set, we also fit the different modelconfigurations to the sea level~~ forcing (Lisiecki and Raymo, 2005) . We keep the Berends curve as a target for global ice volume in the RAMP model, but also include the GMSL reconstruction by Rohling et al. (2022) to have a second target curve. In contrast to Berends et al. (2021a), they used the process modelling approach by Rohling et al. (2021) to deconvolve the sea level signal from the LR04 ~~(Lisiecki and Raymo, 2005) benthic δ^{18}O signal (Rohling et al., 2022)~~stack. Despite their different approaches to reconstructing the ~~global sea level~~ GMSL signal from the LR04 stack, both produce curves in strong agreement with each other, with a mean offset of 3.3 m (Rohling et al., 2022). In the period before 2.6 Ma, the offset is greater. In general, the Berends record is smoother compared to the Rohling record, which arises from a stronger inertia in changes in the ice volume present in the Berends model (Rohling et al., 2022).

2.3 ~~Parameter tuning~~

~~Depending on the configuration, the model has 12 (ORB), 14 (GRAD), 15 (ABR), 16 (RAMP), or 19 (RAMP-l) free parameters. We apply a Monte Carlo method to find an optimal set of parameters for each configuration, similar to the method described by Legrain et al. (2023). Likewise, we use the Python package *emcee* (Foreman-Mackey et al., 2013) which implements the affine invariant ensemble sampler for Markov chain Monte Carlo algorithms, introduced by Goodman and Weare (2010). Due to an increase in numerical efficiency, we use a larger number of walkers, varying between 100 and 500, to explore the parameter space more rigorously. Moreover, instead of using a simple *stretch move* (Goodman and Weare, 2010) as Legrain et al. (2023) have done, we apply a combination of different moves for the proposal. That is, a mixture of 90% *Differential Evolution (DE)* moves and 10% *DE Snooker* moves, as suggested by Ter Braak and Vrugt (2008).~~

~~Furthermore, to verify convergence and escape possible local minima, we also use the Python package *ptemcee* (Vousden et al., 2016; For , which implements parallel tempering in the *emcee* framework. Here, we use 20 different temperatures for the tuning . Another sampler that we implemented is *dynesty* (Speagle, 2020; Koposov et al., 2024) which is a dynamic nested sampling package in Python. This modular approach with multiple different samplers allows for simple switching between the samplers and the most suitable sampler for each new parameterization can be selected to obtain the best results.~~

A most recent work by Clark et al. (2025) deconvolved the Prob-stack (Ahn et al., 2017), a global mean benthic $\delta^{18}O_b$ stack, into its seawater $\delta^{18}O_{sw}$ component, based on ocean temperature data. The ~~Log-Likelihood function for the optimization is defined as:~~

$$\ln \mathcal{L} = -\frac{1}{2} \sum_{i=1}^{N} \left(\frac{\hat{y}_i - y_i}{\sigma} \right)^2 ,$$

~~where $\hat{y}$ is the modelled ice volume, y the target ice volume reconstruction and σ its corresponding standard deviation.~~

2.3 ~~Evaluation of model performance~~

~~The initial conceptual model based on the work by (Legrain et al., 2023) is further refined to include adjustments in its tuning, its parameterization (e.g. time-dependent τ_d parameter, deprecated truncation function) , and the addition of a fourth model configuration (RAMP). To evaluate the effectiveness of these modifications, we conduct identical simulations as described in Legrain et al. (2023). Hence, we run the ORB, ABR, and GRAD models over the past 2 Ma. The resultant root mean square errors (RMSE) between the simulated global ice volumes and~~ Prob-stack was corrected for a long-term increase in $\delta^{18}O_b$, possibly due to a combined effect of diagenesis and the ~~reconstruction by Berends (Berends et al., 2021a) are compared with the originally reported RMSEs (Legrain et al., 2023). Furthermore, we analyze the RMSE of the new RAMP configuration relative to the three original model configurations.~~

~~To evaluate the performance of the four different model configurations, we use the common Bayesian Information Criterion (BIC) (Mitsui and Crucifix, 2017; Mitsui et al., 2022):~~

$$\mathrm{BIC} = -2\ln\mathcal{L}(\hat{\theta}) + K\ln N,$$

~~where K is the number of free parameters used in the model, N the number of data points and $\mathcal{L}(\hat{\theta})$ is the likelihood function of~~ carbonate ion effect. To account for other targets than GMSL, we include the benthic $\delta^{18}O_b$ Prob-stack (Ahn et al., 2017) , as detrended by Clark et al. (2025) and its seawater component $\delta^{18}O_{sw}$ as two further tuning targets for the ~~best model parameters $\hat{\theta}$. The lower the BIC, the better it can describe the observed data points (Mitsui et al., 2022). Parameters that do not significantly improve model performance are penalized in the BIC, such that models that perform equally, but with a lower number of parameters are preferred (Mitsui et al., 2022). The difference in BIC values for two models approximates the Bayes factor for large N (Mitsui and Crucifix, 2017). Hence, the evidence in favour of model i against model$j$ is quantified by the $\Delta\mathrm{BIC}_{ij}$ (Mitsui and Crucifix, 2017):~~

$$\Delta\mathrm{BIC}_{ij} = \mathrm{BIC}_j - \mathrm{BIC}_i.$$

~~As a general rule of thumb (Raftery, 1995; Mitsui et al., 2022), the evidence of model i against model j is considered weak if $0 < \Delta\mathrm{BIC}_{ij} < 2$, positive if $2 < \Delta\mathrm{BIC}_{ij} < 6$, strong if $6 < \Delta\mathrm{BIC}_{ij} < 10$ and very strong if $\Delta\mathrm{BIC}_{ij} > 10$.~~ RAMP model.

3 Results

3.1 ~~Model improvements~~

~~Table ?? presents acomparison of the RMSEs for the three distinct model configurations, as detailed in Legrain et al. (2023), against the results obtained with the new model modifications,i.e. the time-dependent τ_d parameter, the deprecated truncation function and the enhanced tuning procedure. Each of the original model configurations (ORB, ABR, GRAD)is improved by more than 2 m when evaluated over the past 2 Ma. It remains evident that the gradual model continues to exhibit the lowest RMSE, while the orbital model exhibits the largest. Moreover, the newly incorporated RAMP model further reduces the RMSE of the previously superior GRAD model (Legrain et al., 2023) by 2.3 m~~

3.1 RAMP model for Quaternary climate

Tuning the RAMP model to the detrended Prob-stack results in a high correlation between both curves ($R = 0.86$) and an RMSE of 0.22 (Fig. 1a). The model selects a long-lasting increasing trend for the deglaciation parameter in order to reconstruct the target curve. This ramp-like change occurs around 2.2 Ma and lasts until around 500 ka in the model. Furthermore, the RAMP model can correctly identify an increase in the amplitude of $\delta^{18}O_b$ cycles after the MPT. Although some of the post-MPT interglacial peaks are too low in the reconstruction. During the period 1.4 - 1 Ma, the glacial peaks tend to be too low in the RAMP model. Comparing the frequency scalograms of the RAMP reconstruction and its target curve demonstrates close resemblance (Fig. 2a,e). Both curves have a strong ~41 kyr obliquity signal over the entire Quaternary and an emerging ~100 kyr period after around 1 Ma. However, the RAMP reconstruction features some consistent precession signals over the entire simulation period, which are not visible in the benthic target curve.

~~Improved model (this study) results for 2 Myr simulation wrt original model by Legrain et al. (2023). **Model RMSE RMSE Improvement** (2 Myr simulation) (Legrain et al., 2023) (this study) Orbital (ORB) 18.1 16.0 2.1 Abrupt (ABR) 14.4 12.0 2.4 Gradual (GRAD) 13.9 11.7 2.2 Ramp-like (RAMP) NA 11.6 m NA~

3.2 ~~Comparison of the different model configurations~~

~~Figure ?? shows the simulated global ice volume over the past 2.6 Ma for the four different model configurations.~~

~~(i) **ORB model:** The ORB model can identify most of the terminations and endpoints of the interglacials fairly accurately~~ Tuning the RAMP model to the GSML reconstruction, either by Berends et al. (2021a) (Fig. ~~??~~a) ~~. The mean global ice volume over the entire Pleistocene ($\bar{v}$) is 33.5 m for the ORB model and for the Berends reconstruction~~1b) or Rohling et al. (2022) (Fig. 1c) yields similar results. The obtained model-data correlation is high for both curves ($R = 0.86$ and $R = 0.85$). A general ~~trend of increasing glacial global ice volume during the late Pleistocene is also visible, while the amplitude of the~~ bias of too low interglacial peaks for the post-MPT world remains for these targets. The simulated glacial peaks before the MPT persist in being underestimated, especially visible for the Rohling target, which shows larger glacial-interglacial ~~cycles (GICs) stays almost constant. During the first 1 Myr of simulation, the GICs are bounded by -13 m and 43 m with a $\bar{v}$ of 20 m. The last 1 Myr are bounded by 23 m and 75 m with a $\bar{v}$ of 48 m. This corresponds to a trend of almost 30 m in $\bar{v}$ between the early and late Pleistocene. However, the ORB model does not capture the amplitude of~~ variations during this period. While the temporal evolution of $v_0(t)$ for the Berends target closely resembles the one obtained for the ~~GICs correctly. The amplitude stays almost constant throughout the Pleistocene, which is in contrast to the observed increase in amplitude visible in the Berends data. Although for the early Pleistocene, the minima and maxima for the global ice volume during the interglacials and glacials are still similar to the reconstructed ones, they are systematically too large during interglacials and too small during glacial periods. The ORB model cannot produce glacial maxima with more than 75 m of global ice volume. Moreover, most of its interglacials are characterized by weak melting events, which lead to an accumulation of global ice volume over the simulated period. During the last 1 Myr, the global ice volume never fell below 23 m, while the Berends reconstruction exhibits Interglacials with almost 0 m in global ice volume.~~

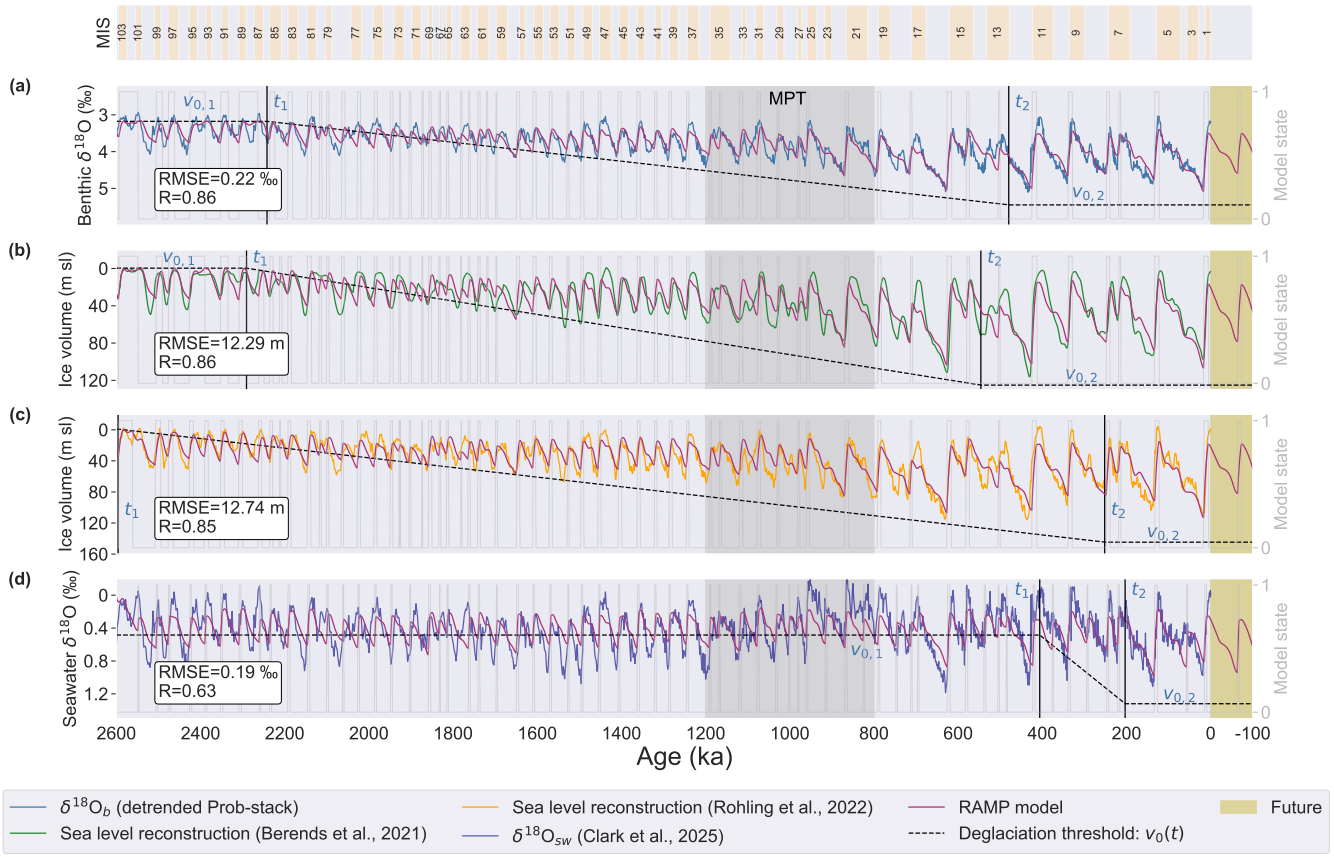

Figure 1. The RAMP model (purple lines) tuned for four different tuning targets: (a) Prob-stack benthic $\delta^{18}O_b$ (Ahn et al., 2017) as detrended by Clark et al. (2025), (b) Berends et al. (2021a) GMSL curve, (c) Rohling et al. (2022) GMSL curve, and (d) Clark et al. (2025) seawater $\delta^{18}O_{sw}$. The vertical black lines indicate the start and endpoint of the ramp and the dotted black lines show the temporal evolution of the deglaciation threshold. The grey-shaded area highlights the classical perspective of where the MPT is located in time. MIS boundaries are given according to Lisiecki and Raymo (2005). Model extrapolations for the future 100 kyr are indicated by the yellow-shaded areas.

~~The projected GICs for the future 250 kyr are visualized in the yellow-shaded area of Fig. **??**a. The ORB model predicts six full glacial cycles for this period. They look similar to the preceding cycles, characterized by small frequencies and amplitudes. Although interglacial melting does not reduce the ice volume below 28 m, the glacial accumulation of the ice volume does not exceed 62 m. $\bar{v}$ for the next~~ benthic target, it does differ for the Rohling GMSL target. For this target, the ramp begins almost immediately in the simulation and lasts longer, extending until approximately 250 ~~kyr is predicted to be 45.9 m with the ORB model.~~

~~Quantitatively, the weak performance of the ORB model can be seen in Table **??**. The coefficient of determination R^2 has the lowest value of 0.47 for the ORB model (2.6 Myr simulation), indicating the lowest correlation with the Berends sea level reconstruction. The same holds for the RMSE, which has the highest value of 17.50 m. Running the ORB model over a shorter~~

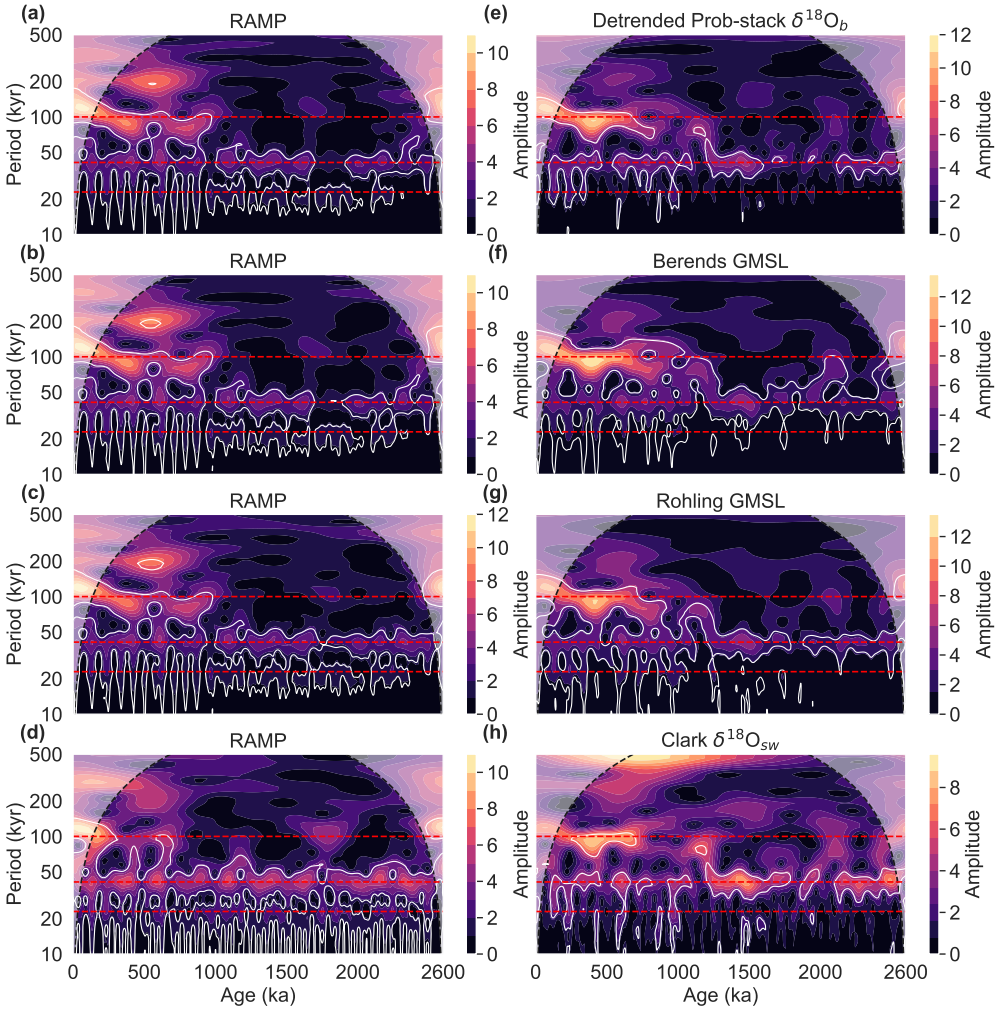

Figure 2. ~~Comparison of~~ Frequency scalograms from the ~~four different model configurations. The simulated ice volume curves are shown~~ continuous wavelet transform for the ~~ORB~~ RAMP model (~~**a**, black curve~~panel (a)~~, ABR~~ (~~**b**, red curve~~d)~~, GRAD~~) and its corresponding tuning targets: (~~**e**~~e) Prob-stack benthic $\delta^{18}O_b$ (Ahn et al., 2017) as detrended by Clark et al. (2025), ~~green~~ (f) Berends et al. (2021a) GMSL curve, (g) Rohling et al. (2022) GMSL curve, and ~~the RAMP model~~ (~~**d**, purple curve~~h) ~~over the whole Pleistocene~~Clark et al. (2025) seawater $\delta^{18}O_{sw}$. ~~Each simulation is plotted over~~ White contours denote significant regions above the ~~ice volume reconstruction by Berends et al. (2021a)~~ red-noise (~~blue curve~~AR1) background at the 95% confidence level. ~~The deglaciation parameter $v_0(t)$~~ Orbital frequencies of precession (~~black dotted line~~~23 kyr)~~is shown for each simulation~~, ~~indicating the internal forcing scenario. The yellow shaded area marks the future 250~~ obliquity (~ 41 kyr) and ~~the respective predictions~~ eccentricity (~ 100 kyr) are marked by ~~each model. The grey-shaded area highlights the classical perspective of where~~ the ~~MPT is located in time. MIS boundaries given according to Lisiecki and Raymo (2005)~~red dotted lines.

~~(2 Myr) or longer (3.6 Myr) period does have a significant effect on its correlation with the Berends data, which is highest for the 3.6 Myr simulation and lowest for the 2.6 Myr simulation. Nevertheless, for all three simulation periods, the ORB model exhibits the worst results.~~

~~Running the ORB model for a reduced duration of 2 Myr (Fig. **??**a) or an extended duration of 3.6 Myr~~ ka. The spectral analysis of both reconstructions (Fig. ~~**??**a) considerably influences the outcomes. The simulated GICs for the 2.6 and 3.6 Myr simulations are characterized by similarly low frequencies and low amplitudes, accompanied by a general trend of increasing global ice volume throughout the simulation period. In contrast, the 2 Myr ORB simulation shows a different picture. The simulated GICs exhibit stronger amplitudes and prolonged periodicities, and the late Pleistocene GICs demonstrate improved alignment with the Berends data. Additionally, a transition from lower to higher frequencies following the MPT is visible, although no detectable shift in amplitude occurs. While some glacial peaks in the early Pleistocene are too strong, certain late Pleistocene glacials are too weak.~~

~~Statistical quantities for the four different model configurations for the three different simulation periods used. Shown are the root mean square error (RMSE), the coefficient of determination (R^2) and the Bayesian information criterion (BIC). **Model RMSE R^2 BIC RMSE R^2 BIC RMSE R^2 BIC** Orbital (ORB) 16.04 0.56 978.5 17.50 0.47 1469.8 15.69 0.64 1389.8 Abrupt (ABR) 12.07 0.75 616.0 12.24 0.74 790.7 12.27 0.78 913.0 Gradual (GRAD) 11.71 0.76 579.1 11.86 0.76 741.7 11.17 0.82 769.4 Ramp-like (RAMP) 11.59 0.77 584.9 11.38 0.78 708.0 10.69 0.83 730.7~~ 2b,c) exhibits the same general patterns as for the benthic target with a dominant obliquity signal, an arising ~100 kyr signal around 1 Ma and a significant precession signal over the entire simulation.

~~(ii) **ABR model:** Introducing a simple abrupt change in the climatic forcing visually improves the reconstructed results of the model quite a lot compared to the ORB model. The timing of the abrupt change in the model parameters $v_0(t)$ and $\tau_d(t)$ (Eq. 8)is another tuning parameter. It was tuned to a value of $t_{abr} = 1246$ ka, visualized as the sudden jump in the deglaciation parameter (black dotted line)in Fig. **??**b. The deglaciation parameter $v_0(t)$ increases from 10.6 m before the jump to 96.8 m afterwards~~Using the seawater $\delta^{18}O_{sw}$ record from Clark et al. (2025) affects the simulation the most (Fig. 1d). For this target, the RAMP model demonstrates the least correlation ($R = 0.63$). In general, while the ~~relaxation time $\tau_d(t)$ increases from -113.3 kyr to 7.0 kyr. There is now a clear distinction between the early and late Pleistocene cycles. While the early ones are characterized by low periodicity and amplitude, they abruptly increase in periodicity and amplitude, following the sudden increase in the deglaciation parameter.~~

~~Before the jump, the GICs are bounded by -8 m and 43 m with a $\bar{v}$ of 21.3 m. After the jump, the GICs are bounded by 1 m and 112 m with a $\bar{v}$ of 44.5 m. This corresponds to an increase of the glacial maxima of almost 70 m. Throughout the Pleistocene, $\bar{v}$ is 33.4 m, which is almost identical to the Berends data. Almost all terminations and interglacial endpoints are correctly identified by the model. An exception is Marine Isotope Stage 35 (MIS35), which is delayed in~~ Berends and Rohling GMSL curves and the ~~ABR model. While the timings of the GICs are well captured in the early Pleistocene, some of the interglacial minima and glacial maximaare underestimated, e.g. MIS 82, MIS 63, MIS 52 and MIS 47. The "double peak" at MIS 15, i.e., the two adjacent minima in global ice volume~~benthic $\delta^{18}O_b$ show a similar pattern over the Quaternary, characterized by lower glacial-interglacial amplitudes prior to the MPT and an increase in peak glacial values, the $\delta^{18}O_{sw}$

curve displays a fundamentally different picture. Here, the glacial-interglacial cycles exhibit much stronger variations in the early Quaternary, and certain of these glacial maxima are comparable in strength to the ones occurring in the late Quaternary. Furthermore, the increasing trend in glacial maxima, apparent for both GMSL curves and the benthic record, is not ~~correctly resolved, as only the first peak is captured. The same holds for MIS 13. While the~~ visible for the seawater $\delta^{18}O_{sw}$. In contrast, it exhibits an increasing period between 2 - 1.5 Ma, followed by a decreasing period in the interval 1.2 - 0.8 Ma. The RAMP model struggles to reconstruct these features. Overall, the glacial-interglacial ~~amplitudes are much better resolved with the ABR compared to the ORB model ,~~ variations are significantly smaller for the ~~general bias of underestimated glacial peaks and interglacial minima remains valid for the late Pleistocene. This can be seen for MIS 17, MIS 16, MIS 12, MIS 11 and MIS 6.~~

~~The ABR model predicts two full glacial cycles over the next 250 kyr~~RAMP reconstruction. While the ~~first cycle is very similar to the preceding one, the latter one is interrupted by a very short interglacial, before the next glaciation continues. These future cycles are bounded by -2 m and 111 m in global ice volume and have a $\bar{v}$ of 49.7 m. The modelled start point of the Holocene is 17 ka and should have ended 4 ka, with the next glacial inception lasting until 105 kyr in the future.~~

~~The ABR model demonstrates a significant improvement in the statistics regarding the alignment between the simulated and the target data, as is evident from Table **??**. The RMSE improves by more than 5 m to a value of 12.24 m and the correlation with the Berends data improves significantly with an R^2 value of 0.74. The strong improvement is also visible for a shorter (2 Myr) or a longer (3.6 Myr) simulation. The ABR model performs similarly well for all three simulation periods, with the best correlation for the longest simulation run.~~

~~Reducing the simulation period to 2 Myr yields similar results~~ pre-MPT glacial extrema are too small, the post-MPT interglacials are too weak. The identified ramp is very limited in time and appears after the MPT in the interval 400 - 200 ka. Hence, it differs substantially from the long-lasting patterns observed for the previous three targets. Moreover, the RAMP model fails in reconstructing the post-MPT 100 kyr cycles (Fig. **??**~~b) . The abrupt MPT is delayed to 1094 ka. The pre-MPT GICs continue to be dominated by low amplitude and low periodicity. The abrupt jump in the deglaciation threshold leads to a clear shift towards smaller frequencies and larger amplitudes. Instead of two full glacial cycles over the next 250 kyr, the ABR model now forecasts three full glacials of intermediate strength, in close agreement with the prediction by the RAMP model. On the other hand, a prolonged simulation period of 3.6 Myr leads to worse results (Fig. **??**b). While the timing of the MPT is consistently located at 1163 ka and the post-MPT cycles are similar, the pre-MPT cycles have changed significantly. Similarly to the GICs produced by the ORB model, their amplitude and period are too small. In contrast to the ORB model, the increasing trend of global ice volume is not linear, but shows a multi-millennial cyclic pattern. The future cycles are shorter in period and of smaller amplitude, such that there are four GICs forecasted over the next 250 kyr. Hence, future predictions of the ABR model are highly inconsistent and always depend on the simulation period.~~

~~(iii) **GRAD model:** In contrast to the abrupt change in internal forcing, implemented in the ABR model, the GRAD model incorporates a gradual transition throughout the Pleistocene. This change in internal forcing further improves the match between the simulated and the target data, as can be seen in Fig. **??**c. The simulated global ice volume curve is in very good agreement with the Berends reconstruction. Over the course of the Pleistocene, the deglaciation parameter $v_0(t)$ increases from 20.1 m to 126.4 m and the relaxation time $\tau_a(t)$ decreases from 19.8 kyr to 5.2 kyr . During the first 1 Myr of the simulation,~~

the GICs are bounded by -2 m and 52 m with $\bar{v}$ of 19.5 m. For the 2d) correctly. It only features a 100 kyr signal for the last 1 Myr, this transitions to bounds of 1 m and 118 m with $\bar{v}$ of 49.2 m. During the simulation period, the mean global ice volume $\bar{v}$ is 33.5 m, which is in agreement with that of Berends. ~200 kyr, after the ramp-like change in $v_0(t)$.

As is the case for the ABR model, the GRAD model can correctly detect most terminations and interglacial endpoints. Even MIS 35 is captured, but an artificial intermediate glacial is added. Some of the weaker interglacials, such as MIS 23, are missed, as is the case for the ABR model . Moreover, the interglacial double peak during MIS 15 is now captured, due to the cost of extending the subsequent glacial MIS 14 too much. The amplitude of pre-MPT GICs increases, leading to better reconstructions, especially visible for GICs in the interval 1.6 - 1.2 Ma. Following the MPT, certain glacial maxima continue to be underestimated. This is particularly evident in the cases of MIS 16, MIS 12, and MIS 6. Similarly, some interglacial minima are not consistent with the Berends reconstruction. This is particularly the case for MIS 31 (demonstrating improvement relative to the ABR model) and MIS 17, while MIS 11 now aligns well with the Berends reconstruction. The tuned parameter values are very similar for the two GMSL targets and the detrended Prob-stack (SI Tab. S3). This highlights that the RAMP model, as discussed above, yields robust outputs for these three tuning targets. While the $\delta^{18}O_{sw}$ target differs more significantly in its parameter values, certain parameters like $\alpha_{Fsi}, \alpha_O, \alpha_g$ and $v_{0,1}$ remain similar.

The GRAD model projects two complete glacial cycles within the forthcoming 250 kyr. Both cycles exhibit a substantial amplitude of ~ 110 m and have a periodicity of 100 kyr. The initial future GIC is nearly identical between the ABR and GRAD models. However, while a minor interglacial phase disrupts the second GIC in the ABR model, Extrapolating the RAMP model yields consistent results for all four tuning targets. For the Berends and Rohling GMSL curves and the detrended Prob-stack, the GRAD model omits this interglacial period, resulting in the formation of a second pronounced glacial phase. These future cycles are bounded by -1 m and 113 m in global ice volume and have a $\bar{v}$ of 52.2 m. The Holocene started 16 RAMP model simulates the end of the Holocene at 6 ka and the subsequent glacial cycle to reach its maximum at 64 kyr in the future. The $\delta^{18}O_{sw}$ target results in almost the same timings with an endpoint for the Holocene at 10 ka and ended 1 ka. The proceeding glacial cycle would last until 108 a next glacial maximum at 63 kyr in the future. future. For all four targets, the RAMP model underestimates the current interglacial lowstands and projects an intermediate, strong future glaciation, compared to the previous ones.

In comparison to the ABR model, The extended simulation period and the different tuning targets prevent a direct comparison between the RAMP and the GRAD model demonstrates better agreement between the modelled and the target data, evidenced by L23 models. Hence, we run the RAMP model for a reduced simulation period of 2 Myr and tune it to the Berends GMSL curve. A comparison with the GRAD model, which is the best-performing model version of L23, demonstrates better model-data agreement with a reduction in its RMSE by 0.38 m, resulting in a value of 11.86 m. Furthermore, its R^2 metric exhibits a slight increase, reaching a value of 0.76. The same holds for longer and shorter simulation periods. While the 2 Myr and 2.6 Myr simulations yield very similar results, the prolonged 3.6 Myr run correlates the closest to the Berends data.

The GRAD model yields very consistent results if run for 2 Myr RMSE of more than 1 m, while relying on three parameters less, but still providing more information on the temporal change in $v_0(t)$. A complete comparison with all L23 model versions and the new RAMP model is shown in the SI (Fig. **??**c) or for 3.6 Myr (Fig. **??**). The MPT can be reproduced for all three

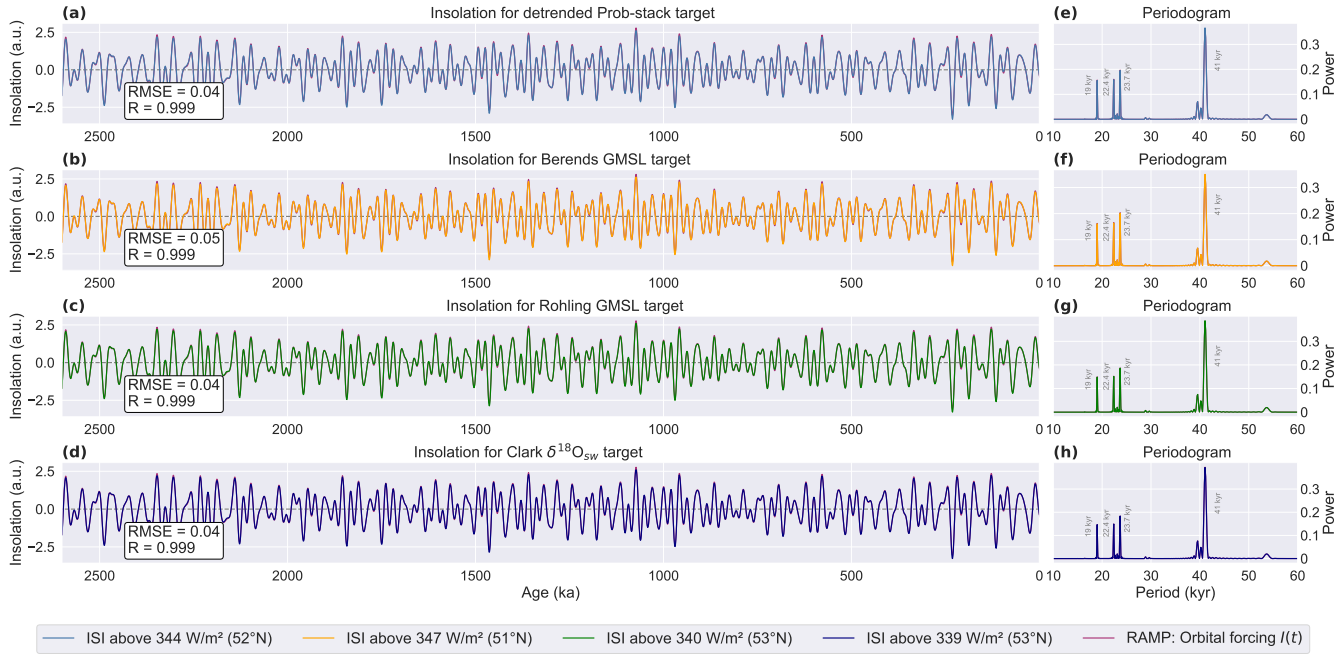

Figure 3. Comparison of the orbital forcing in the RAMP model (purple line), when tuned for the **(a)** Prob-stack (Ahn et al., 2017) as detrended by Clark et al. (2025), **(b)** Berends et al. (2021a) GMSL reconstruction, **(c)** Rohling et al. (2022) GMSL reconstruction and **(d)** Clark et al. (2025) $\delta^{18}O_{sw}$ decomposition. For each forcing curve, the best-fitting insolation curve is shown. ISI curves were calculated by code from Leloup and Paillard (2022). The RAMP model was tuned to the detrended Prob-stack. Panel **(e)**-**(h)** show the corresponding periodogram of both forcing curves.

simulation periods. The GRAD model consistently forecasts 2 strong glacial cycles over the next 250 kyr when run for 2 or 2.6 Myr, whereas the ice volume for the 3.6 Myr simulation diverges after 110 kyr in the future. S1, Tab. S2).

(iv) **RAMP model:** In comparison to the GRAD model, the RAMP model features a gradual trend in internal forcing only over a fixed period, i.e. it features a ramp-like forcing scenario. The onset of the ramp occurs at $t_2 = 2159$ ka, concluding at $t_1 = 858$ ka. Before and after the ramp, the deglaciation parameter $v_0(t)$ and the relaxation time $\tau_d(t)$ remain constant, while during the ramp, they exhibit a linear increase and decrease, respectively. While $v_0(t)$ increases from an initial value of -12.9 m to a final one of 98.4 m, $\tau_d(t)$ decreases from 31.4 kyr to 6.3 kyr. The first 1 Myr of simulation yields GICs between -1 m and 41 m with $\bar{v}$ of 19.4 m. During the last 1 Myr of simulation, the GICs shift towards bounds of 0 m and 114 m with $\bar{v}$ of 48.5 m. The global mean ice volume over the entire Pleistocene corresponds to a $\bar{v}$ of 33.5 m, in perfect agreement with Berends, as already the case for the GRAD model. In general,

3.2 Orbital forcing in the RAMP model

The temporal evolution of the quantity $v(t)$ in the RAMP model is externally driven by the orbital forcing $I(t)$. It is based on a linear combination of the precession parameter and obliquity (Eq. 3). The two associated tunable model weights α_{Esi} and α_{O} determine how the orbital forcing in the RAMP model looks ~~very similar to the GRAD model, as can be seen in Fig. ??d. The most remarkable difference concerns future predictions.~~

~~As for the GRAD model, the timings of terminations and glacial endpoints are captured very well~~ and how strong the precession and obliquity signals are. Figure 3 shows the resulting orbital forcings for the RAMP model~~. Some general biases remain, which were already present in the GRAD model. For example, MIS 14 remains too long, leading to a delayed MIS 13, the glacial maxima of MIS 12, MIS 10 and MIS 6 are underestimated, whereas certain interglacial minima are not reached, as for MIS 31, and MIS 17.~~

~~The most obvious difference between the GRAD and~~ , when tuned for each of the four different tuning targets. To identify the insolation curve corresponding to the obtained $I(t)$ curve, we compare it to daily insolation curves at specific latitudes, monthly averaged ones, and various integrated summer insolations (ISI) [1]. The insolation values are taken from La2004 orbital solution (Laskar et al., 2004). Insolation curves and orbital forcing in the RAMP model ~~is concerning the simulated GICs for the next 250 kyr. While the GRAD model predicts two strong glacial cycles,~~ are normalized for comparison.

The tuned weights (α_{Esi},α_{O}) for the orbital forcing in the RAMP model ~~anticipates three intermediate glaciations.They are characterized by glacial periods between 60 and 80 kyr and are delimited by 6 m and 83 m with $\bar{v}$ of 43.4 m. In the RAMP model, the Holocene lasted from 16 ka until 1 ka. The proceeding glaciation would continue till 65 kyr in the future.~~

~~Table ?? indicates that the RAMP model shows the best agreement with the Berends data out of the four different model configurations. It lowers the RMSE compared to the GRAD model by nearly half a meter, resulting in a value of 11.38 m. Its correlation with the Berends data improves to the highest value of 0.78. The situation is the same for the 2 Myr and the 3.6 Myr runs, where the RAMP model consistently yields the best results among all models.~~

~~The RAMP model produces very consistent results when run for a shorter (2 Myr, Fig. ??d) or a longer (3.6 Myr,~~ exhibit a remarkable similarity across all four targets (SI Tab. S3). Consequently, it is unsurprising that the obtained orbital forcings for these targets closely resemble one another, leading to a similar identification of the insolation curves with the highest correlation (Fig. ~~??d)period. While the onset of the ramp is always tuned to an early stage of the simulation ($t_2 = 1{,}884$ ka for 2 Myr simulation; $t_2 = 2{,}159$ ka for 2.6 Myr simulation; $t_2 = 3{,}479$ ka for 3.6 Myr simulation), the end is always located between 600 and 900 ka ($t_1 = 664$ ka for 2 Myr simulation; $t_1 = 858$ ka for 2.6 Myr simulation; $t_1 = 840$ ka for 3.6 Myr simulation). Compared to the other models, the RAMP model uniquely provides consistent projections of future glacial cycles, predicting the occurrence of three intermediate glacial cycles over the next 250~~ 3a-d). For the four targets, the closest correlation is found with the ISI above a threshold ranging from 339 to 347 $\mathrm{W\,m^{-2}}$, at latitudes between 51° and 53° N, indicating an almost perfect alignment ($R \geq 0.998$). The spectral analysis (Fig. 3e-h) of these insolation curves demonstrates that they consist of a

[1] The integrated summer insolation (ISI) was introduced by Huybers (2006) and is defined as the sum of insolations on days exceeding some threshold τ:

$$\mathrm{ISI}(\tau) = 86{,}400 \cdot \sum_i \beta_i W_i,$$

where W_i is the mean insolation in W/m^2 on day i, and $\beta_i = 1$ if $W_i \geq \tau$ and 0 otherwise.

dominant obliquity peak around 41 kyr, accompanied by pronounced precession peaks occurring around 19 kyr, 22.4 kyr and 23.7 kyr.

~~To investigate how a different tuning target affects the simulation outcome, the four models are tuned to the Rohling sea level curve (Rohling et al., 2022) instead of the Berends data (Fig ??, Fig ??) . The different tuning target affects the outcome of the ORB model the most. When tuned to the Rohling data, the ORB model simulates GICs with larger amplitudes and extended periods. It is in closer agreement with the results obtained for the 2 Myr run, compared to the 2.6 and 3.6 Myr runs. However, the ORB model is still incapable of reconstructing the MPT, since there is no change in the amplitude and frequency of the GICs throughout the simulation .~~

~~For the ABR model , the different tuning target affects the simulation outcome only slightly. For the Rohling-based solution, the double peak during MIS 15 isreconstructed and the model now predicts three intermediate strong GICs for the upcoming 250 kyr, in very close agreement with the RAMP predictions. The timing of t_{abr} is tuned to 1098 ka, a slightly younger age compared to the Berends-based simulation.~~

~~As visible from supplementary Fig. ??c, the simulated global ice volume over the past 2.6 Ma for the GRAD model is barely affected by the chosen tuning target. The main difference is that the post-MPT interglacial minima are consistently lower for the Rohling-based simulation. For the next 250 kyr, the forecasted timings and amplitudes of the GICs are in very close agreement.~~

~~Similarly to the GRAD model,~~

3.3 Model sensitivity

We conduct several experiments to assess the sensitivity of the RAMP to initial conditions, the robustness of the ~~RAMP model demonstrates minimal impact when the tuning target is switched from the Berends data to the Rohling data~~ glacial patterns to changes in model parameters and simulation time and how robust the model tuning is. To investigate the model sensitivity, we use the optimal parameter set (SI Tab. S3) for the RAMP model when tuned for the detrended Prob-stack, keeping all parameters fixed except one. The first parameter that we vary, v_i, sets the initial value for the quantity $v(t)$ (Fig. ~~??d). A notable difference lies in the earlier onset of the ramp ($t_2 = 2286$ ka), while the end stays similar ($t_1 = 881$ ka). However,~~ 4a). Lower initial values of 0%, 50%, 90% and 95% of the optimal value converge to the ~~different timings do not appear to influence the simulated GICs, nor the projected future cycles. Therefore,~~ same output in less than 200 kyr. Similarly, higher values of 105%, 110%, 200% and 1000% converge to the same output in less than 200 kyr. This demonstrates that the RAMP model ~~stands out as the sole model providing consistent outcomes across all three evaluated simulation periods and for a different tuning target~~is not sensitive to the choice of initial conditions.

3.4 ~~Spectral analysis of the different models~~

~~Potential frequency shifts due to the MPT can be seen in the periodograms in~~ The second parameter that we vary is the model threshold v_1, which we alter in an interval of $\pm 10\%$ ($[0.9, 0.95, 1, 1.05, 1.1] \cdot v_{1,\text{best}}$) (Fig. ~~??. The Berends data exhibits a dominant 41 kyr peak when analyzed on a timeframe of 2.6 - 0.8 Ma, which transitions to a combination of a minor 41 kyr~~

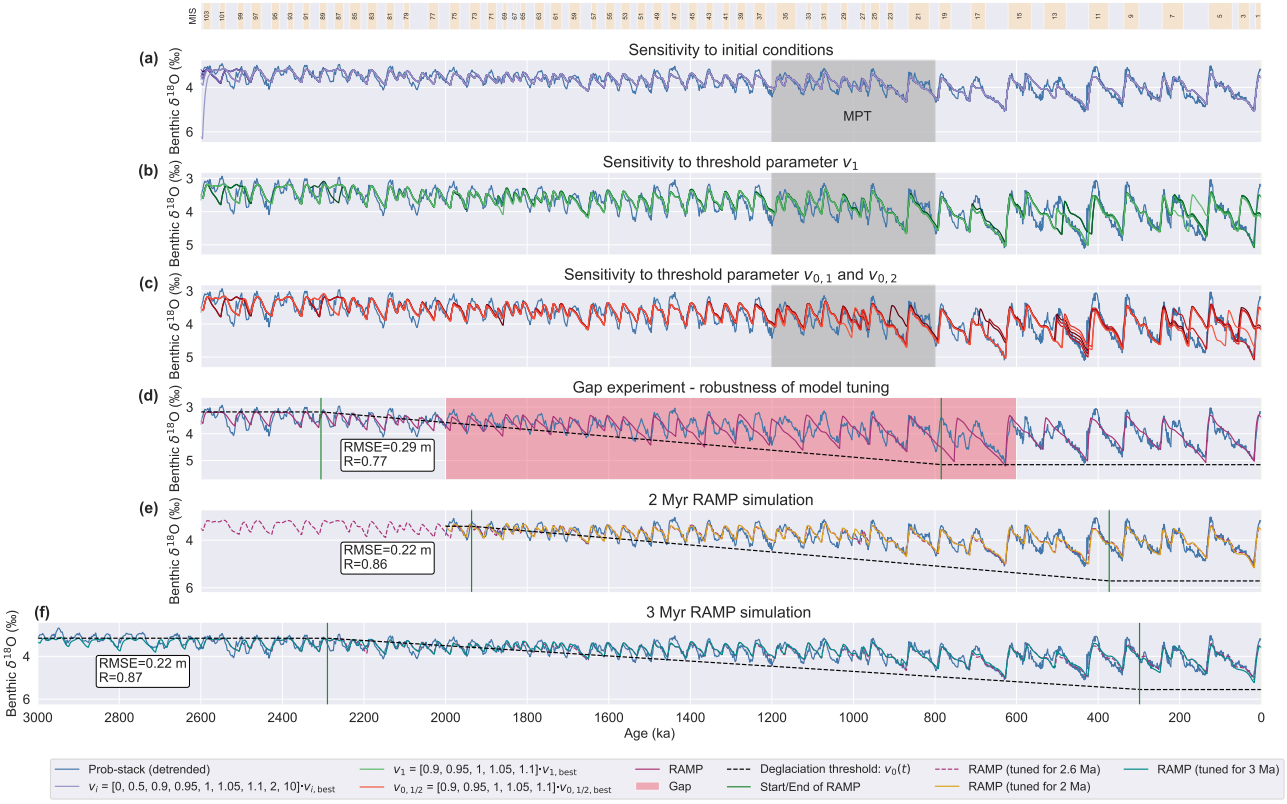

Figure 4. Parameter sensitivity in the RAMP model. **(a)** Sensitivity to initial conditions: v_i (initial quantity) is varied within $[0, 0.5, 0.9, 0.95, 1, 1.05, 1.1, 2, 10] \cdot v_{i,best}$ (purple lines). **(b)** Sensitivity to model threshold: v_1 is varied within $[0.9, 0.95, 1, 1.05, 1.1] \cdot v_{1,best}$ (green lines). **(c)** Sensitivity to model thresholds: $v_{0,1}$ and $v_{0,2}$ are simultaneously varied within $[0.9, 0.95, 1, 1.05, 1.1] \cdot v_{0,1/2,best}$ (red lines). **(d)** Robustness of the model tuning. The RAMP model was tuned for the detrended Prob-stack, starting from a unit vector and excluding the period 2 - 0.6 Ma (red-shaded area) from the tuning target. **(e)** RAMP model when tuned for a 2 Myr run (golden line) compared to the standard 2.6 Myr tuned version (purple dotted line). **(f)** RAMP model when tuned for a 3 Myr run (cyan line) compared to the standard 2.6 Myr tuned version (purple dotted line). The blue line shows the detrended Prob-stack. The grey-shaded area highlights the classical perspective of where the MPT is located in time. MIS boundaries are given according to Lisiecki and Raymo (2005).

~~and a dominant 100 kyr peak for the last 800 ka. The ORB model does not feature such a transition in periodicity with a 41 kyr period being dominant in both analysis timeframes. In contrast, the other three models exhibit a distinctly different pattern. All three models demonstrate a clear change in periodicity, transitioning from a dominant 41 kyr cyclicity in the early- to mid-Pleistocene towards a combination of a minor 41 kyr and a dominant roughly 100 kyr period~~4b). While most of the glacial cycles remain unchanged, some specific stages seem to be more sensitive to parameter changes. This is ~~in good agreement with the Berends reconstruction. The peak around 100 kyr for the last 800 ka in the ABR model is slightly larger compared to the GRAD and RAMP models, which agrees better with the Berends reconstruction.~~

In summary, the ABR, GRAD and RAMP models are capable of reproducing a shift in periodicity due to the MPT in good agreement with the results obtained from the Berends data. On the other hand, the ORB model is the only model configuration that is incapable of reproducing a change in frequency.

Lomb-Scargle Periodogram of the four different models (coloured solid lines) and of the Berends sea-level reconstruction (blue dashed lines). Panel **(a)** - **(d)** display the periodogram during the early- and mid-Pleistocene (2.6 - 0.8 Ma), while panel **(e)** - **(h)** show the late-Pleistocene (0.8 Ma to present). Minimum frequency: $f_{min} = 150^{-1}$ kyr^{-1}, maximum frequency: $f_{max} = 10^{-1}$ kyr^{-1}.

3.4 Model performance

To further quantify the performance of each model and to identify the importance of adding certain parameters to the model, we focus on the ΔBIC values. Table **??** provides a complete summary of all ΔBIC values between the four models for the three different simulation periods. It can be seen that the ORB model performs the worst for all three simulation periods, despite having the least number of parameters (12). The ABR model contains three additional parameters (15) which significantly improve the performance of the model. It exceeds a ΔBIC of more than 300 for all three simulation periods compared to the ORB model, indicating very strong evidence in favour of the ABR model. In addition to smaller RMSEs (see Table **??**) , the GRAD model has one parameter less (14)than the ABR model. As a result, the GRAD model outperforms the ABR model, as indicated by ΔBIC values of 36.9, 49.0 the case for the early Quaternary, around 2.5 and 143.6 for the three different simulation runs. Despite having two additional parameters compared to the GRAD model, the RAMP model (16) shows better performance over simulation periods of 2.6 Myr and 3.6 Myr. Only for a reduced simulation period of 2 Myr the ΔBIC value becomes negative, indicating positive evidence in favour of the GRAD model. This result is reflected in the small difference between their RMSEs (see Table **??**) for the 2 Myr simulation, while the difference in RMSEs becomes larger for longer simulation periods. For the 2.6 Myr and 3.6 Myr simulations, its ΔBIC calculated with respect to the GRAD model is greater than 30, indicating very strong evidence in favour of 2.3 Ma. Thereafter, all simulations converge to the same pattern and only differ for the late Quaternary glacial cycles. Apparently, the interglacial double peaks observed during Marine Isotope Stage (MIS) 13 and MIS 7 are particularly sensitive to changes in parameters, and failing to detect these accurately can lead to an early termination of the RAMP modellast glacial period.

The last sensitivity test that we perform concerns the deglaciation threshold $v_0(t)$. Here, we vary simultaneously $v_{0,1}$ and $v_{0,2}$ in an interval of $\pm 10\%$ ($[0.9, 0.95, 1, 1.05, 1.1] \cdot v_{0,1/2,\text{best}}$) (Fig. 4c).

In summary, the analysis of This produces a similar result as for the Bayesian information criterion underlines the finding that the ORB model performs significantly worse than the other three models. While the GRAD model is superior to sensitivity to the v_1 parameter. Only early Quaternary cycles around 2.5 and 2.3 Ma are affected, while the simulated glacial cycles till around 1 Ma remain unchanged. The 100 kyr world is more sensitive to changes in the $v_{0,1/2}$ parameters, with MIS 13 and MIS 7 being particularly sensitive.

To assess the robustness of the model tuning, the ABR modelRAMP model is tuned from a unit vector (i.e. initial parameter guess of 1 for all parameters) to the detrended Prob-stack, excluding the time interval from 2 to 0.6 Ma from the target dataset.

Consequently, the RAMP model ~~outperforms all other models, except for a reduced simulation period of 2 Myr, when the evidence for the GRAD model is positive.~~

~~ΔBIC values between all four models for the three simulation periods used.~~ ~~**Model # Parameters ΔBIC vs ORB ΔBIC vs ABR ΔBIC vs GRAD ΔBIC vs ORB ΔBIC vs ABR ΔBIC vs GRAD ΔBIC vs ORB ΔBIC vs ABR ΔBIC vs GRAD**~~

~~Orbital (ORB) 12 0 / / 0 / / 0 / / Abrupt (ABR) 15 362.5 0 / 679.1 0 / 476.8 0 / Gradual (GRAD) 14 399.4 36.9 0 728.1 49.0 0 620.4 143.6 0 Ramp-like (RAMP)16 393.6 31.1 -5.8 761.5 82.7 33.7 659.1 182.3 38.7~~

3.4 ~~The MPT in the RAMP model~~

~~The RAMP model produces an almost abrupt change in the amplitude and frequency of glacial cycles after around 900 ka, despite having a gradual change in internal forcing. To understand how a gradual change in forcing can produce a sudden change in global ice volume dynamics, it is important to investigate how the mechanisms for triggering deglaciations and glaciations have changed during this period. This transition for the period of 1.2~~ is only tuned for the early Quaternary (2.6 ~~- 0.6 Ma is shown in~~ 2 Ma) and the late Quaternary (last 600 ka), without any information on the glacial cycles during the gap period. The reconstructed benthic δ^{18}O curve closely aligns with the target curve (Fig. ~~**??**.~~

~~As outlined in the Methods section, two conditions must be fulfilled to trigger a deglaciation (Eq. 6)and two conditions for the onset of a new glaciation (Eq. 7). A termination is triggered once the ice volume exceeds a critical volume (black line) and the current insolation is sufficiently large~~ (4d). In comparison with the reconstructed curve tuned to the complete target (Fig. 1a), the exclusion of the gap results in a reduction of the R value from 0.86 to 0.77. The indicated ramp period remains extended with an earlier onset at ~ 2.3 Ma (previously ~ 2.2 Ma) and an earlier end at ~ 800 ka (previously ~ 500 ka). Despite lacking any information on the glacial cycles during the gap period (red-shaded ~~areas). Once both conditions hold (purple dots) , a state change from a glaciation to a deglaciation mode is performed and the dynamics of the system follow Eq. (5). This is the case until two criteria are fulfilled: Firstly, the ice volume falls again below a critical volume (black line; note the inverted y-axis~~ area in Fig. ~~**??**), and secondly, the insolation is sufficiently small (blue-shaded area). This allows the model to enter the next glacial state (red dots), and its evolution follows Eq. (4).~~

~~As apparent in Fig. **??**, there is an abrupt change in amplitude and frequency of the glacial cycles after glacial termination TXIII. Before this termination, each or every second insolation peak resulted in a deglaciation. After TXIII, more insolation peaks were missed, leading to extended glacial periods and amplitudes. Termination TXIII was triggered by a strong insolation peak and led to a very short preceding glacial period. Due to the short glacial period, only a small global ice volume was accumulated. Subsequently, the interglacial led to the lowest global ice volume (12.6 m) in the last 400 ka. In the~~ 4d), the RAMP model ~~, the deglaciation threshold (black line) increases over time, due to the increase of the~~ can accurately reconstruct the timings of most glacial terminations. This demonstrates the robustness of the applied model tuning and the overall robustness of the RAMP model in accurately reconstructing glacial cycles without having any prior knowledge about them.

Finally, we alter the simulation period to verify the robustness of the glacial patterns and whether the identified ramp period changes. When we tune the RAMP model ~~parameter $v_0(t)$ (black dotted line). Therefore,~~ for a reduced period of 2 Myr to the detrended Prob-stack and compare it with the ~~required critical ice volume to trigger the next termination increases as well. The~~

combination of the low global ice volume at the onset of the next glacial period after TXIII and the increasing deglaciation threshold in the RAMP model enabled the model to skip three insolation peaks to yield the first glacial maximum exceeding 80 m in global ice volume and led to the longest glacial period in the Pleistocene so far. After TXIII, the extended periodicities and amplitudes prevailed.

Simulated ice volume by the RAMP model (blue line) for the period 1.2 - 0.6 Ma, together with its deglaciation and glaciation thresholds. The forcing curve $I_k(t)$ is shown in red. While the red shaded area marks values above the model threshold v_1, the blue shaded area marks values below. The time-dependent deglaciation parameter $v_0(t)$ is represented by the black dotted line, while the solid black line indicates the deglaciation threshold. The purple dots indicate terminations, and the red dots mark glacial inceptions. Modelled terminations are labelled with Roman numerals.

3.4 Performance of the RAMP-l model

The RAMP-l model includes three additional parameters which make the forcing term $\tilde{I}_k(t)$ ice volume dependent. This significantly improves the simulation outcomes (Fig. **??**a). The RMSE, compared to the standard RAMP model , is improved by 1.36 m to a new optimal value of 10.02 m. Likewise, R^2 increases to a new best value of 0.83. The improved performance comes with the cost of adding three new parameters to the model. Despite these extra parameters, the calculation of the ΔBIC between the RAMP-l and RAMP models demonstrates with a value of $\Delta \mathrm{BIC}_{\mathrm{RAMP\text{-}l,RAMP}} = 107.3$ that there is very strong evidence in favour of the RAMP-l model over 2.6 Myr tuned version of the RAMP model.

The simulated global ice volume by the RAMP-l model can be seen in , both curves almost perfectly align for the past 2 Myr (Fig. **??**a. While the early onset 4e). The end of the ramp stays similar for the RAMP-l model ($t_2 = 1978$ ka), the endpoint is shifted by over occurs slightly later in the Quaternary (around 400 kyr ($t_1 = 454$ ka)compared to the RAMP model. Therefore, the total duration ka instead of 500 ka). The onset of the ramp is extended. The deglaciation parameter $v_0(t)$ increases from an initial value of 20.7 m to a final value of 127.4 m. The relaxation parameter $\tau_d(t)$ decreases from 41.2 kyr to 5.3 kyr during the Pleistocene. During the first 1 Myr, the simulated global ice volume is confined to values between -4 m and 48 m with a mean ice volume of 19.8m. The last 1 Myr are characterized by an ice volume between -1 m and 111 m and a mean ice volume of 47.9 m. The global mean ice volume over the entire Pleistocene corresponds to a $\bar{v}$ of 33.3 m, in very close agreement with the Berends data.

Compared to the standard RAMP model, the RAMP-l model simulates interglacials with smaller ice volumes, and glacial with larger ones. Hence, bounded to 2 Ma, due to the interglacial-glacial variability is increased. This is in better agreement with the Berends data, especially visible for the GICs in the interval 1.6 - 1.2 Ma. Another major difference is that the RAMP-l model no longer resolves the two interglacial double peaks (MIS15, MIS7), but in turn, the succeeding glacial (MIS14)is better resolved. reduced simulation period. However, the optimal value for the onset ($t_1 = 1936$ kyr) lies very close to this upper bound, indicating that t_1 might exceed this upper bound, as it does for the 2.6 Myr run.

A further difference to the standard RAMP model concerns the simulated GICs for the next 250 kyr. While the RAMP model projects three intermediate strong glacials, We repeat the same experiment, but for an extended simulation period of 3 Myr (Fig. 4f). Over the past 2.6 Myr, both curves align almost perfectly. Without an upper bound of 2 Ma for t_1, as in the previous

simulation, the RAMP-1 model projects, similar to the GRAD model , the occurrence of two complete glacial cycles within the next 250 kyr. Both cycles exhibit major glaciations of ~110 m and have glacial periods of around 100 kyr. The Holocene started 15 ka and would continue for the next model tuning finds a very similar pattern for the temporal shape of the ramp for the 3 kyr. The following glacial termination would be 107 kyr in the future.

Figure **??** shows that the periodograms for the simulated ice volume by the RAMP-1 model and the ice volume reconstruction by Berends et al. (2021a) are in close agreement. Although the early to mid-Pleistocene GICs (Myr run and the 2.6 -0.8 Ma) are mainly driven by a ~ 41 kyr periodicity (Fig. **??**b), the late Pleistocene (last 0.8 Ma) GICs show a combination of ~ 41 kyr and 100 kyr periods with a dominant peak around ~ 100 kyr (Fig. **??**c).

(a) Simulated global ice volume by the RAMP-1 model (golden line) over the whole Pleistocene, together with the ice volume reconstruction by Berends et al. (2021a) (blue line). The black dotted line shows the deglaciation parameter $v_0(t)$. The yellow shaded area marks the future 250 kyr and the respective model predictions. The grey-shaded area highlights the classical perspective of where the MPT is located in time. The periodograms of both ice volume curves are shown for the time interval 2.6 Ma - 0.8 Ma **(b)** and for the time interval 0.8 Ma - present **(c)**. Minimum frequency: $f_{min} = 150^{-1}$ kyr^{-1}, maximum frequency: $f_{max} = 10^{-1}$ kyr^{-1}.

3.4 Forcing in the RAMP-1 model

In the model, Myr run. The 3 Myr run results in an onset of the ramp at around 2.3 Ma (previously 2.2 Ma) and an end at around 300 ka (previously 500 ka). Hence, altering the simulation period for the RAMP model does not largely affect the simulated glacial patterns, and the external driver of the temporal evolution of the ice volume is the orbital forcing I_α. It is composed of a linear combination of three orbital parameters, namely: obliquity, precession, and phase-shifted precession. The three tuning parameters α_{Esi}, α_{Eco} and α_{O} determine how this linear combination adds up and Fig. 3a shows the resulting orbital forcing in the RAMP-1 model. To identify the insolation curve corresponding to the obtained I_α curve, we compare it to daily insolation curves at specific latitudes, monthly averaged ones, and various integrated summer insolations (ISI) reported in the literature. The closest correlation is found with the ISI above 285 at 67° N (calculations done by code provided in Leloup and Paillard (2022)). Both curves align almost perfectly (Fig. 3a) with an RMSE of 0.24 m and an R^2 value of 0.94. The spectral analysis (Fig. 3b) of these insolation curves demonstrates that they consist of minor precession peaks around 19 kyr, 22.4 kyr and 23.7 kyr and a dominant obliquity peak around 41 kyrlong-lasting trend obtained for the ramp is a robust feature for all simulation periods.

(a) Orbital forcing I_α (Eq. 4, 5) in the RAMP-1 model (orange line) together with the best fitting insolation curve, the ISI above 285 at 67° N (blue line, calculated by code from Leloup and Paillard (2022)). **(b)** Periodogram of both insolation curves.

4 Discussion

The second forcing term in the RAMP-1 model does not drive the time evolution of the ice volume directly , as the I_α term does. Instead, it controls the associated thresholds (Eq. 6, 7) to initiate state changes in the model. This forcing is the $\tilde{I}_k$ term.

~~Due to its ice volume dependency, its amplitude increases over time (Fig. **??**a). Hence, with the progression of the Quaternary period, an increase in global ice volume corresponds with a rise in the $\tilde{I}_k(t)$ term. While in the early Quaternary, the forcing is confined to values between $\pm$ 25 m, it increases towards values exceeding $\pm$ 50 m in the late Quaternary. The first threshold condition requires $\tilde{I}_k(t)$ to exceed or fall below the model threshold v_1.~~

4.1 Ramp-like change for GMSL and benthic δ^{18}O targets

Conceptual models like the RAMP model cannot shed light on the underlying physical mechanisms directly (~~red-shaded or blue-shaded areas, respectively, in Fig. **??**a). The forcing term also affects the deglaciation threshold ($v_0(t) - \tilde{I}_k(t)$). A spectral analysis of the forcing term shows that the dominant frequency has shifted during the Quaternary. The $\tilde{I}_k(t)$ term is always composed of precession peaks at 19 kyr, 22.4 kyr and 23.7 kyr and an obliquity peak around 41 kyr. However, while in the early Quaternary (~~e.g. whether a long-term trend in v_0 is due to regolith removal or a gradual CO_2 decrease, etc.), since they do not include the involved physical or chemical processes directly. However, their strength lies in their capability to investigate the underlying temporal structure of such a change. The advantage of the new ramp formulation is that the RAMP model incorporates multiple scenarios for the temporal change in the deglaciation parameter, particularly all those discussed in Legrain et al. (2023) (ORB, ABR, GARD). By tuning the model to a paleoclimatic target curve, it selects the most appropriate temporal structure for $v_0(t)$. For three out of the four targets used in this study (both GMSL curves and the detrended Prob-stack), the RAMP model shows a similar pattern, namely a long-lasting increasing trend in $v_0(t)$, which started between 2.2 and 2.6 ~~Ma - 1.2 Ma), the dominant peak was the obliquity one, it shifted in the late Quaternary (0.8 Ma~~ Ma and ended between 250 - ~~present) towards dominant precession peaks at 22.4 kyr and 23.7 kyr (Fig. **??**b, c).~~

~~Given that $\tilde{I}_k(t)$ undergoes temporal changes, it is interesting to investigate how this impacts the state changes in the model. For this reason, we identify each time step t_i in the simulation in which a state change occurs. These time steps are visualized in Fig. **??**d, colour-coded with the current model state. While an interglacial state is followed by a glacial inception in the next simulation step, a glacial state is followed by a glacial termination. At least one of the two necessary conditions (for termination: Eq. 6, for gl.inception: Eq. 7) was not fulfilled in the previous time step t_{i-1}. Hence, we classify the time steps t_i according to~~ 500 ka. Hence, for these targets, the ~~decisive condition that finalized the state change, i.e. the condition related to v_1 (for termination: $\tilde{I}_k(t) \geq v_1$, for gl. inception: $\tilde{I}_k(t) < v_1$), related to $v_0(t)$ (for termination: $v(t) + \tilde{I}_k(t) > v_0(t)$, for gl. inception: $v(t) + \tilde{I}_k(t) \leq v_0(t)$), or both conditions are fulfilled simultaneously. The pattern in Fig. **??**d shows a regime change around 1.7 Ma in the model regarding the decisive condition for triggering a state change. Before 1.7 Ma, glacial terminations and inceptions are mainly timed by the v_1 condition, i.e. when the $\tilde{I}_k$ term falls below or exceeds the v_1 threshold. In contrast, after 1.7 Ma, each interglacial state is terminated by the next glacial inception due to the v_1 condition and each glacial state ends in a termination due to the~~ RAMP is not in favour of an abrupt change, a rather short and limited change (e.g. which only lasted during the MPT) or no change in $v_0(t)$, which would correspond to a purely orbitally driven climate. These findings agree with the results of the L23 models, where the authors identified a gradual trend over the entire 2 Myr-long simulation period to be more likely than an abrupt one or a purely orbital one. The strength of the RAMP model is that it gives information about a potential start and end of such a gradual change. The L23 GRAD model was only run for the past 2 Ma, therefore, it

does not allow earlier changes in v_0~~condition (three exceptions where~~ , but the RAMP model reveals that the change in v_0 ~~and v_1 conditions are simultaneously fulfilled) . Hence,~~ likely started even before 2 Ma. An alternative approach is presented in Ganopolski (2024), where the author prescribes the change in the ~~glacial terminations are timed by crossing some critical ice volume.~~

~~**(a)** Forcing $\tilde{I}_k(t)$ in the RAMP-l model (Eq. 9) and model threshold v_1 (red line). One condition to trigger a termination is that $\tilde{I}_k(t)$ needs to exceed the threshold v_1 (red-shaded area, Eq. 6). Conversely, a necessary condition for glacial inception is that $\tilde{I}_k(t)$ is below v_1 (blue-shaded area, Eq. 7). The yellow shaded area marks the future 250 kyr. **(b)** The periodogram of the forcing term $\tilde{I}_k(t)$ for the interval 2.6 Ma - 1.2 Ma. **(c)** The periodogram of the forcing term $\tilde{I}_k(t)$ for the interval 0.8 Ma - present. **(d)** Decisive condition for triggering a state change. The coloured dots mark time steps when a state change occurs in the model. Blue dots indicate that the model is currently in a glacial state and will experience a glacial termination in the next time step. Conversely, red dots indicate that the model is currently in an interglacial state and will experience a glacial inception in the next time step. To change from a glacial to an interglacial state, or vice versa, two conditions, including the model parameters $v_0(t)$ and v_1, must be fulfilled (Eq. 6,7). The y-axis marks which of these two conditions was the decisive one (last one that was fulfilled) to trigger a state change, or in rare occasions when both conditions were fulfilled at the same time step.~~

4.2 ~~Sensitivity of large ice sheets to precession in the RAMP-l model~~

~~During the tuning process, the following values were found for the l-parameters:~~

$$l_{\mathrm{Esi}} = 0.68, \qquad l_{\mathrm{Eco}} = 0.14, \qquad l_{\mathrm{O}} = 0.14.$$

~~Hence, for large ice volumes, the precession term $l_{\mathrm{Esi}} v(t) \mathrm{Esi}(t)$ isdominant. This can also explain the apparent shift towards dominant precession peaks (Fig. **??**b,c) in the late Quaternary when the amplitude of glacials increased.~~ critical ice volume parameter v_c (similar to our v_0) with a hyperbolic tangent, which closely resembles the temporal evolution of the regolith-free area as described in Willeit et al. (2019). This shows that the regolith-free scenario can reproduce the MPT, but since it relies on a single prescribed temporal structure for this change in v_c, it gives no information on how likely such a temporal structure is.

~~To investigate the sensitivity of large ice sheets to~~ The RAMP model challenges the possibility that orbital forcing alone could explain the MPT. Despite the flexibility of using different linear combinations of precession and obliquity ~~, it is convenient to separate the forcing term $\tilde{I}_k(t)$ (Eq. 9) in two terms, one including all precession and~~ (even when including co-precession~~terms and the other containing all obliquity terms:~~

$$\tilde{I}_{k,Pr}(t) = [k_{\mathrm{Esi}} + l_{\mathrm{Esi}} v(t)]\,\mathrm{Esi}(t) + [k_{\mathrm{Eco}} + l_{\mathrm{Eco}} v(t)]\,\mathrm{Eco}(t)$$

$$\tilde{I}_{k,Ob}(t) = [k_{\mathrm{O}} + l_{\mathrm{O}} v(t)]\,\mathrm{Ob}(t)$$

$$\tilde{I}_k(t) = \tilde{I}_{k,Pr}(t) + \tilde{I}_{k,Ob}(t)$$

~~For the last 900 ka,)~~, tuning the RAMP model did not result in a scenario where $v_0(t)$ remained constant, but always increased over the Quaternary, i.e. implying that an internal change in the ~~larger l parameter for precession leads to larger amplitudes in the precession term $\tilde{I}_{k,Pr}(t)$ compared to the obliquity term $\tilde{I}_{k,Ob}(t)$ (Fig. **??**a).~~

~~To investigate the sensitivity of large ice sheets to orbital forcing, we focus on the triggering of glacial terminations during the past 900 ka in the RAMP-l model (Fig. **??**b).Glacial terminations are triggered once $\tilde{I}_k(t)$ exceeds v_1 and the sum of the current forcing and ice volume $v(t) + \tilde{I}_k(t)$ exceeds $v_0(t)$. As previously shown in Fig. **??**d, the decisive condition for glacial terminations for the last 1.7 Ma is~~ system is required to reconstruct the MPT. In contrast, there are recent studies linking the occurrence of the ~~v_1 condition. This means that the timing of these glacial terminations is determined by the timing when the critical ice volume threshold is crossed. For the last 900 ka, almost all terminations are associated around peak $\tilde{I}_k$ forcing conditions (purple dots in Fig **??**b). An exception is MIS15, when a strong minimum in forcing allowed to build up such a large ice volume that the next moderately positive forcing values were sufficient to trigger a termination. During the last 900 ka, 11 terminations occurred. Figure **??**a demonstrates that for 10 out of those 11 terminations, the precession term of the forcing was larger than the obliquity one. Hence, the precession term $\tilde{I}_{k,Pr}$ played the key role in achieving the required forcing to end glacial periods during the past 900 ka.~~

~~**(a)** The two components of the forcing term $\tilde{I}_k(t)$: precession and co-precession components $\tilde{I}_{k,Pr}(t)$ (purple line, Eq. 9) and the obliquity components $\tilde{I}_{k,Ob}(t)$ (green line, Eq. 9). Their respective values at glacial terminations are marked with coloured dots. **(b)** Simulated ice volume by the RAMP-l model (golden line) for the past 900 ka, together with its deglaciation and glaciation thresholds. The forcing $\tilde{I}_k(t)$ is shown in red. While the red shaded area marks forcing values above the model threshold v_1, the blue shaded area marks values below. The time-dependent deglaciation parameter $v_0(t)$ is represented by the black dotted line, while the solid black line indicates the deglaciation threshold. The purple dots indicate terminations, and the red dots mark glacial inceptions.~~

5 ~~Discussion~~

4.1 ~~Using only orbital forcing~~

~~The four standard models (ORB, ABR, GRAD, RAMP) are conceptualisations of four distinct forcing scenarios. The ORB simulation represents a climate system influenced solely by orbital forcing, excluding any internal feedback mechanisms. Our results showed that this approach fails in reconstructing the MPTalong with its associated change in amplitude and frequency. This could already be observed in the ORB model of Legrain et al. (2023), which simulates glacial amplitudes before the MPT that are consistently too high, while those after the MPT are too low. Moreover, a clear transition from 41 kyr to 100 kyr cycles is not observed. In contrast, a pronounced 200 kyr signal during the period of 1-2 Ma is visible,~~ MPT to orbital forcing alone. Ma et al. (2024) introduce the *integral of annual mean insolation anomaly* (IAMIA), which quantifies successive small step-wise insolation changes over a given period of time. The authors show that IAMIA exhibits a large shift around 935 ka, which they hypothesise to have enabled the onset of the MPT. Another recent preprint by Verbitsky and Omta (2025) discusses the idea that the MPT is due to a delayed relaxation process, which can lead to an abrupt-like jump in the dominant period.

This shift in periodicity can be highly sensitive to the initial conditions, and the ~~41 kyr signal intensifies in the late Pleistocene, almost matching the power of the 100 kyr signal.~~

~~We cannot exclude the possibility that different orbital background conditionsor a different parameterization could recreate the MPT. However, our ORB model supports the idea that orbital changes alone cannot account for this major climatic transition. This suggests the presence of non-linearities within the climate system that modify Earth's response to changes in~~ sensitivity depends on the amplitude of the orbital forcing. ~~This conclusion aligns with findings from other studies (Clark et al., 2006; Lelou~~ ~~.~~

4.1 ~~Abrupt versus gradual scenario~~

~~If a purely external driver for the MPT can be ruled out, it remains open whether the MPT was triggered by an abrupt or a gradual scenario. Although improving the model performance did not alter the general finding of Legrain et al. (2023) that the model is in favor of a gradual transition, the ABR model does reproduce the MPT, and the timing of its modelled abrupt change (1.25 Ma) agrees with some proxy reconstructions. While some climatic marine records indicate an abrupt transition approximately 0.9 Ma (Elderfield et al., 2012; Yehudai et al., 2021), the modelled jump in the ABR model is more consistent with the proxy records from Site U1537, which show an abrupt change in dust deposition around 1.25 Ma (Weber et al., 2022).It also corresponds to the onset of gradual cooling trends evident in multiple sea-surface temperature (SST) records (McClymont et al., 2013) . Moreover, it aligns with a study by Nyman and Ditlevsen (2019) that claims that the MPTdid not lead to a stationary 100 kyr world, but rather that there was an abrupt transition from ~41 kyr to ~ 80 kyr cycles about 1.2 Ma, followed by a gradual increase towards 120 kyr thereafter~~Although our model yields a contrasting view, we cannot exclude the possibility that a different orbital parameterization, e.g. IAMIA, could recreate the MPT.

~~Although the ABR model can reproduce the MPT, the obtained results with the GRAD model are better. The GRAD model shows an increasing secular trend in the deglaciation parameter over the entire Quaternary. While the superior performance of the GRAD model is in favour of~~ While the RAMP model supports a long-lasting gradual trend in the ~~climate~~ Earth-climate system, its underlying physical mechanism cannot be directly inferred but just hypothesized since the conceptual modelling approach lacks the physical representation of these mechanisms. Whether a gradual erosion of regolith (Clark and Pollard, 1998; Clark et al., 2006), a gradual decrease in atmospheric CO_2 ~~(Berends et al., 2021b; **?**)~~(Berends et al., 2021b; Scherrenberg et al., 2025) , some sea-ice feedback mechanism, a mixture of these (Willeit et al., 2019) or something else, is the underlying mechanism behind this trend, requires a more physics-based model which can explicitly resolve these mechanisms.

The hypothesis of a long-term decrease of atmospheric CO_2 concentrations as the cause of the MPT remains difficult to verify since the continuous direct CO_2 records from Antarctic ice cores are currently limited to the past $\sim$ 800 ka (Willeit et al., 2019; Bereiter et al., 2015) and beyond that, the discontinuous ice core samples from the Allan Hills Blue Ice area provide only ~~three~~ snapshots of direct CO_2 estimates ~~attached to a large uncertainty (Yan et al., 2019)~~of the last 3 Ma, attached larger uncertainties (Peterson et al., 2024; Yan et al., 2019). CO_2 estimates over the pre-MPT and the MPT worlds can be obtained using indirect proxies inferred from terrestrial and marine archives. For ~~instance~~example, CO_2 reconstructions are based on δ_{13}~~C carbonates~~ ^{13}C from leaf-wax (Yamamoto et al., 2022), from paleosols (Da et al., 2019), or ~~δ^{11}B boron based~~ boron

isotope-based reconstructions (Chalk et al., 2017; Hönisch et al., 2009). Based on the latter, there ~~seems~~ appears to be a decrease in minimal CO_2 concentrations during glacial maxima ~~across~~ throughout the MPT. However, looking into a recent synthesis compiling all proxy-based paleo CO_2 data ($CenCO_2PIP$ Consortium, 2023), alternative CO_2 reconstructions suggest different trends. Hence, there is no clear answer yet regarding the long-term evolution of the atmospheric CO_2 concentration across the Pleistocene.

However, this knowledge gap is anticipated to be addressed in the future through ongoing efforts to retrieve a continuous ice core record extending beyond one million years, as pursued, for instance, by the European Beyond EPICA-Oldest Ice Core project and the Australian Million Year Ice Core project.

4.1 ~~Ramp-like internal forcing~~

~~On top of the ABR and GRAD models, we implemented another forcing scenario, the RAMP model, characterized by a time-limited linear trend between two constant states. Unlike the ABR and GRAD models, it is more flexible since it does not determine the internal forcing a priori. The tuning process aims to find the most likely parameters to obtain the best agreement with the target data. If the start and endpoints of the ramp are the same, or very close, the RAMP model simulates an abrupt change in the internal system, similar to the ABR model. Conversely, if these points are positioned at the beginning and end of the simulation period, the RAMP model simulates a linear trend in the climate system across the entire Quaternary, similar to the GRAD model. Thus, tuning the RAMP model facilitates the evaluation of the relative significance of these two scenarios without prior assumptions. Moreover, it allows identifying a start point, an endpoint and the duration of a possible linear trend in the climate system. By tuning the RAMP model, we found that a long-lasting linear trend of increasing deglaciation parameter $v_0(t)$ and decreasing relaxation time $\tau_d(t)$ yields the best results. For the two simulations run for Quaternary climate (2 Myr and 2.6 Myr), we found that the onset of the ramp occurs early, around 2 Ma and the end around 600 - 900 ka. The tuned RAMP model demonstrated greater relevance than the GRAD and ABR models (for 2.6 Myr and 3.6 Myr simulations), suggesting that a gradual trend within the Quaternary, that lasted over a limited period, is key to reproducing the MPT.~~

As Verbitsky and Crucifix (2023) point out, while some phenomenological models can very accurately recreate observational time series (i.e. paleo records), it does not necessarily reflect their physical similarity to ~~Nature~~nature. Hence, it is crucial to investigate whether such a ramp-like ~~forcing in our RAMP model can be~~ scenario in the model is justified by paleo records or more sophisticated modelling studies. A ~~review study by McClymont et al. (2013) investigated the imprint of the MPT on the surface ocean through the analysis of various SSTrecords. They found that most sites do exhibit a pronounced cooling trend over the period 1.2 - 0.8 Ma, but regional differences exist, especially regarding the magnitude of the cooling and the onset of the cooling trend, starting as early as 1.8 Ma. An analysis of Atlantic and Pacific benthic $\delta_{13}C$ as proxies for obliquity and precession responses in Atlantic overturning revealed a major transition which occurred 1.6 -~~ synthesis of globally distributed sea surface temperature (SST) records by Clark et al. (2024) found that two long-term cooling stages occurred during the last 4.5 Ma. The first started around 4 Ma, which was followed by a second period of intensified cooling between 1.5 ~~Ma (Lisiecki, 2014).~~

Ma and around 0.8 Ma. Thereafter, temperatures stabilised for the late Pleistocene. A statistical model by Tzedakis et al. (2017) relates glacial terminations with a required energy threshold and shows that this deglaciation threshold had to rise over the Pleistocene. They found that the increase is ramp-like with a linear trend lasting from 1.55 Ma until 0.61 Ma. The conceptual model by Ganopolski (2024) can also recreate the MPT by changing its critical ice volume parameter ramp-like rather than linear. However, it uses a smoother transition function, namely a hyperbolic tangent centered around 1050 ka with a transition time of 250 kyr. The asymptotic ~~behavior~~ behaviour of the hyperbolic tangent leads to quasi-constant parameter values prior to 1.55 Ma (twice the transition time) and after 0.55 Ma. The author stresses the similarity with the modelled regolith mask in Willeit et al. (2019), connecting the ramp-like structure with the erosion of the Northern Hemisphere regolith. The optimal volcanic CO_2 ~~outgasing~~ outgassing scenario (V2) found in Willeit et al. (2019) resembles a ramp-like structure for the past 2.6 Ma with a decreasing trend of volcanic CO_2 ~~outgasing~~ outgassing between around 2.1 Ma and 0.9 Ma.

In summary, ~~the various proxy records differ remarkably in their temporal structure and range from abrupt climatic transitions and prolonged gradual trends to time-limited gradual transitions. Certain proxy records, when considered alongside the modelling studies presented above,~~ certain proxy records and modelling studies support the concept of a ramp-like internal ~~forcing. The modelled endpoint~~ change. Reaching a constant value for $v_0(t)$ in the RAMP model~~(0.6-0.9 Ma)~~ , after a long increasing trend, aligns with findings from SST records (∼0.8 Ma, ~~McClymont et al. (2013)), abrupt climatic transitions visible in certain records (∼ 0.9 Ma, Elderfield et al. (2012); Yehudai et al. (2021)~~Clark et al. (2024)), a statistical model of energy thresholds (∼0.6 Ma, Tzedakis et al. (2017)) and with a modelled volcanic CO_2 outgasing scenario (∼ 0.9 Ma, Willeit et al. (2019)). ~~In contrast, the early onset of the gradual trend in~~ , where stable conditions were reached in the late Quaternary, although the endpoint for the RAMP model (0.25 - 0.5 Ma) occurs later. The volcanic CO_2 outgassing scenario in Willeit et al. (2019) closely resembles the temporal structure in the RAMP model (for Berends GMSL and detrended Prob-stack) with an early onset around ~~2 Mais less evident in the proxy records, as only laterstarting points are visible. The earliest onset of a long-lasting~~ 2.1 Ma. On the other hand, the first cooling trend in ~~SSTs was identified around 1.8 Ma(McClymont et al., 2013), while a major transition in the Atlantic overturning was detected around 1.6 -~~ global SST records appears earlier (4 Ma), and the intensified cooling trend around 1.5 Ma ~~(Lisiecki, 2014)~~appears later than the one in the RAMP model. Moreover, the ramp-like energy threshold in Tzedakis et al. (2017) also suggests a later start around 1.55 Ma. ~~The volcanic CO_2 outgasing scenario in Willeit et al. (2019) closely resembles the ramp-like structure in our RAMP model with an early onset around 2.1 Ma. However, atmospheric CO_2 concentrations as a potential source for our ramp-like forcing cannot be tested considering the large uncertainty of proxy-based reconstructions across the Pleistocene (as already discussed in Sect. **??**). This knowledge gap is anticipated to be addressed in the future through ongoing efforts to retrieve a continuous ice core record extending beyond one million years, as pursued, for instance, by the European Beyond EPICA-Oldest Ice Core project and the Australian Million Year Ice Core project.~~

4.1 ~~Sensitivity of large ice sheets~~

~~In the second part of this study, we selected the best-performing model (i.e.~~

4.1 Seawater $\delta^{18}O_{sw}$

Besides the detrended benthic δ^{18}O Prob-stack, its deconvolution into seawater $\delta^{18}O_{sw}$ is included in the RAMP model as a new target. This recent deconvolution by Clark et al. (2025), based on an ocean temperature data compilation, gives a contrasting view compared to the Berends and Rohling deconvolutions. It exhibits a decline in $\delta^{18}O_{sw}$ during the MPT, interrupting a previous period of increasing values and showing larger glacial-interglacial amplitudes in the early Quaternary, with certain of these glacial maxima comparable in strength to the ones occurring in the late Quaternary. This contrasting view led to a failure of the RAMP model ~~) and adjusted it to test if an ice volume dependency in the threshold's forcing term could further improve this new model (RAMP-1). This allows testing the sensitivity of large ice sheets to changes in orbital parameters. This model adjustment significantly improved the performance, compared to the four standard models, demonstrating that the thresholds (introduced in Eq. 6, 7) used in the base modelsmight be too simplistic to model the entire Quaternary accurately and that it requires additional adjustments like an ice volume dependency to account for changes in the underlying climate system over the course of the Quaternary.~~ in accurately matching the target curve and in reconstructing the MPT. The RAMP formulation seems to be less suited for this target, as apparent from the selected ramp period (400 - 200 ka). However, a final reconstruction of this $\delta^{18}O_{sw}$ record into a GMSL curve is not yet available.

~~Recent studies suggest that the duration and timing of deglaciation and glaciation events over the last 900 ka were largely deterministic and driven by the relative phasing of precession, obliquity, and eccentricity (Barker et al., 2022, 2025). Barker et al. identified candidate precession peaks, which are precession peaks that begin while obliquity is increasing, as essential for glacial terminations. They found that glacial terminations during the last 900 ka correspond to the first candidate precession peak after a minimum in eccentricity.Meanwhile, obliquity seems to play a more important role in maintaining peak interglacial conditions and for glacial inceptions.While obliquity seems to play a more important role in the direct evolutionary equations in the RAMP-1 model,~~

4.2 Next glacial cycle

While neglected in many conceptual models, extrapolating the next glacial cycle can be an important tool of model evaluation, since this represents the only time interval in which a model cannot be tuned or fitted onto some existing paleoclimatic target curve. Since the extrapolated curves lack anthropogenic CO_2 emissions, they must be interpreted as baseline experiments of how the glacial cycles would evolve in the absence of anthropogenic impacts. More complex models, coupled to the ~~picture is different for triggering glacial terminations. During the last 900 ka,~~ carbon cycle, project, even without any anthropogenic influence, an unprecedentedly long Holocene, lasting for another 50 kyr (Ganopolski et al., 2016; Talento and Ganopolski, 2021) . In contrast, the RAMP model projects for all four tuning targets that the next glacial cycle has already started 6 - 10 ka and will last until around 64 kyr in the future. In their recent study, investigating the influence of precession and obliquity on glacial interglacial cycles, Barker et al. (2025) estimate that the current interglacial conditions would last for 11 ~~terminations occurred in the RAMP-1 model , out of which 10 were dominated by the precession term.Hence, our RAMP-1 model supports the idea that precession plays a more important role for glacial terminations of the last 900 ka, as proposed by Barker et al. (2025)~~kyr.

when obliquity reaches its next minimum and the succeeding glacial would be interrupted in around 66 kyr (again neglecting anthropogenic effects). Other conceptual models similarly predict a contrasting view for the next glaciation: Calder (1974) projected a start 5 ka and an end in around 119 kyr (see his Fig. 2), Imbrie and Imbrie (1980) estimated a start 6 ka (see their Fig. 7) and Figure 5 in Paillard (2015) reveals that only a large enough glaciation threshold can lead to a prolonged Holocene in the P98 model, while a lower threshold would have terminated the Holocene already a few kyr ago. While other models like the L23 models, Model 3 of Ganopolski (2024) and the Leloup and Paillard (2022) model were not extrapolated for the next glacial cycle, it can be expected that they would yield similar results as the RAMP model (i.e. a short Holocene), since they are based on similar model dynamics. Therefore, the RAMP characteristic of simulating a prolonged Holocene is a striking feature which is also present in other conceptual models or studies. The discrepancy with the more sophisticated models might be due to the missing carbon feedback in these models or due to the choice of the glaciation threshold in the RAMP model, which only depends on orbital forcing or parameters.

~~Presumably, while precession seems to be more important for glacial terminations, obliquity appears to be more important for the time evolution.~~

4.3 Role of precession and obliquity

While we cannot directly investigate the physical effects of precession and obliquity in the climate system with the RAMP model, we can investigate their influence on the dynamics of the model. By using a linear combination of precession and obliquity rather than a single insolation metric, we can explicitly see which roles these two orbital quantities play in the model. For instance, this allows us to investigate the spectral power of the obtained orbital forcing in the RAMP model.

The evolution of the ~~ice volume in the RAMP-l~~ quantity $v(t)$ in the RAMP model is driven by a linear combination of ~~three~~ two orbital parameters: precession ~~, co-precession~~ and obliquity. Therefore, the orbital forcing in the model depends on the tuned parameter values α_{Esi} and α_{O}. In comparison to other conceptual models, which rely on a specific insolation metric for the orbital forcing (e.g. Ganopolski (2024); Paillard (1998); Leloup and Paillard (2022)), this allows for more flexibility in the model and reduces subjective modelling choices. ~~This approach~~ A similar approach with three orbital parameters has been successfully used in other models (Imbrie et al., 2011; Legrain et al., 2023). Choosing a specific insolation metric does affect the quality of the reconstruction result due to variations in their spectral profiles (Leloup and Paillard, 2022). For instance, the insolation at ~~the~~ summer solstice at 65° N has a stronger precession signal than the one obtained from the caloric ~~season insolation. Hence, selecting an insolation curve to force the modelled ice volume can pose a modelling bias. Furthermore~~summer insolation at 65° N (as introduced by Milankovitch (1941)).

Moreover, since using a linear combination of ~~orbital parameters can reproduce most~~ precession and obliquity can accurately reconstruct various insolation curves at different latitudes and seasons ~~(Imbrie et al., 2011; Loutre, 1993), the tuned parameters will construct~~ (SI Sec. 4), the tuning process will select an optimal curve for the orbital forcing. This optimal forcing ~~term~~ curve can then be compared to real insolation curves. ~~For the RAMP-l~~ In addition, available conceptual models use a variety of orbital forcings, e.g. Model 3 (Ganopolski, 2024) uses the maximum summer insolation at 65° N, P98 relies on the same metric, but with an artificial truncation function added, Tzedakis et al. (2017) use the caloric summer insolation at 65° N. Regarding this

variety of different orbital forcings in use, it is of interest to see which metric the RAMP model selects. For the RAMP model, we found that the tuned ~~parameters result in a curve which is in almost perfect agreement ($R^2 = 0.94$) with the ISI above 285~~ orbital weights ($\alpha_{\mathrm{Esi}}, \alpha_{\mathrm{O}}$) are almost the same for all four tuning targets and hence are the orbital forcings $I(t)$. For all four targets, we find that the curve with the highest correlation ($R \geq 0.998$) is the ISI above a threshold ranging from 339 to 347 $\mathrm{W\,m^{-2}}$~~at 67~~, at latitudes between 51° and 53° N. ~~This curve has a very strong obliquity signal, indicating that for the evolutionary term $\frac{\mathrm{d}v}{\mathrm{d}t}$, the obliquity signal is more important than the precession one~~These curves consist of a dominant obliquity peak and substantial precessional signals. This contrasts with the widely used insolation curve at summer solstice at 65° N, which exhibits dominant precession signals and a reduced obliquity signal. However, it therefore better resembles the precession-obliquity imprint of the caloric summer insolation curve.

4.4 ~~Future predictions~~Model limitations

~~Another feature of the conceptual models presented in this study is their ability to extrapolate future glacial-interglacial cycles. For the next 250 kyr, the GRAD and RAMP-1 models predict two full glacial cycles with amplitudes of ~ 110 m sl. On the other hand, the standard RAMP model predicts three intermediate strong glacials. Since these models do not account for CO_2, and thus do not include anthropogenic climate change, these results can only be considered as baseline experiments of how the glacial cycles would evolve without the anthropogenic effect of rising atmospheric CO_2. Besides the ORB model~~ The RAMP model depends on a specific threshold choice to switch between a glaciation and a deglaciation state. Köhler and van de Wal (2020) challenge this binary view of interglacials and glacials. By classifying interglacials based on the absence of substantial NH land ice outside of Greenland, they found that the classification of interglacials, especially in the early Quaternary, is ambiguous. This classification depends on the defined threshold and the choice of the underlying record. This perspective questions the ability of any threshold-based, ~~all other models located the start of the Holocene between 15-17 ka and its end around 4 ka in the past and 3 kyr in the future. This early end of the Holocene does not align with results from other models coupled to the carbon cycle, which project,without any anthropogenic effect, that the current interglacial conditions will last for approximately another 50, 000 years (Ganopolski et al., 2016; Talento and Ganopolski, 2021). However, a slightly reduced pre-industrial atmospheric CO_2 concentration of 240 ppm instead of 280 ppm could have led to a new glacial inception that started already a couple of thousand years ago (Ganopolski et al., 2016). Excluding anthropogenic CO_2 emissions and extrapolating their analysis of candidate precession peaks, Barker et al. (2025) found that the next glacial inception would reach a maximum rate during the next 11kyr and should be terminated around 66 kyr in the future. This is in close agreement with the RAMP model, which predicts the next glacial termination in 65 kyr, while the ABR, GRAD and RAMP-1 model all predict the next glacial termination in 105 to~~ two-state model to unambiguously classify interglacial states. Therefore, the identified glacial and deglacial states in our model should only be carefully considered in combination with the applied thresholds, defined in Eq. 6,7, and for the used target record (benthic δ^{18}O, sea-water δ^{18}O or global ice volume).

Available global mean sea level data exhibit large uncertainties. Between 50 and 30 ka, geological and geochemical reconstructions of GMSL vary up to 60 m and above (Farmer et al., 2023). Model-based deconvolutions of global δ^{18}O into GMSL, like for the Berends et al. (2021) and Rohling et al. (2022) sea level reconstructions, exhibit similar large uncertainties. While the Berends

curve shows an LGM lowstand of around 100 m, the Rohling curve gives around 108 ~~kyr, which is in closer agreement with the prediction of ~ 110 kyr by Talento and Ganopolski (2021)~~m. Both values are well below observational-based reconstructions of around 130 - 135 m for the LGM (Austermann et al., 2013; Lambeck et al., 2014; Yokoyama et al., 2000). Furthermore, the Berends and Rohling reconstructions, although differing in their modelling approaches, both rely on the LR04 benthic δ^{18}O stack, whose age model was orbitally tuned. Hence, the chosen reconstruction depends on the orbital tuning applied to the LR04 stack. Consequently, the simulated global ice volume in the RAMP model has to be interpreted in light of the large uncertainties already present in the target data.

5 Conclusions and outlook

In this study, we constructed ~~an improved~~ a new conceptual model of ~~Quaternary global ice volume, including four different internal forcing scenarios, alongside another modelconfiguration, designed to test the sensitivity of large ice sheets in the late Quaternary. We showed that the RAMP-1 model~~ the Quaternary global climate, the so-called RAMP model. It improves the previous L23 models of Legrain et al. (2023) by reducing the number of parameters in the model (2-4 less), reducing the model-data mismatch (ΔRMSE > 1 m), including three new paleo records as target (Rohling GMSL, $\delta^{18}O_b$, ~~which incorporates a ramp-like internal forcing and an ice volume dependency in its threshold forcing, is the best-performing model. It is in favour of a long-lasting linear trend in the climate system rather than an abrupt change or a purely orbitally driven model . The optimal insolation metric for the~~ $\delta^{18}O_{sw}$), increasing the numerical efficiency (speedup of ~30), refining the tuning strategy, extrapolating the model ~~is~~ for the ~~ISI above 285 at 67° N, demonstrating the importance of the obliquity signal for the evolutionary equations. It also suggests that large ice sheets in the late Quaternary (last 900 ka)~~next glacial cycle and implementing a more flexible ramp-like parameterization, which includes all former L23 temporal scenarios. The model is insensitive to the initial conditions, i.e. the initial value of $v(t)$. While the early Quaternary cycles are less sensitive to changes in the threshold parameters ($v_{0,1/2}, v_1$), the late Quaternary ones are more sensitive~~to precession than obliquity and, therefore, more important in triggering glacial terminations. In addition, the RAMP and RAMP-1 simulations yield a very early onset for the gradual trend around 2 Ma. This finding emphasizes the importance of intensifying the work to obtain an even older continuous ice core record than the recently drilled ~ 1.2 Myr old ice from the European Beyond EPICA-Oldest Ice Core project~~, particularly the appearance of interglacial double peaks around MIS 13 and MIS 7. The model tuning is very robust and can yield consistently good results, even when large parts of the tuning targets are excluded. Reducing or extending the simulation period does not largely affect the simulated glacial cycles, and the identified long-term change in the deglaciation parameter is a very robust feature in the model.

The RAMP model yields consistent results for three tuning targets (Berends GMSL, $\delta^{18}O_b$, $\delta^{18}O_{sw}$). They all result in a long-lasting increasing trend in the deglaciation parameter, which started in the early Quaternary (2.6 - 2.2 Ma) and lasted until 250 - 500 ka, in order to reconstruct the MPT. The model fails in reconstructing the recent deconvolution of the Prob-stack into $\delta^{18}O_{sw}$, which fundamentally differs from prior deconvolutions. The RAMP consistently projects a short Holocene, which already ended a few kyr ago, followed by an intermediate strong glacial, lasting until around 64 kyr in the future. For all

tuning targets, the RAMP model consistently selects a very similar orbital forcing curve, which is in close agreement with the ISI above a threshold ranging from 339 to 347 $\mathrm{W\,m^{-2}}$, at latitudes between 51° and 53° N, which are all characterized by a dominant obliquity peak and substantial precession signals.

At the moment, the ~~conceptual models presented in this work only rely on orbital parameters~~ RAMP model only relies on precession and obliquity as an input~~and they output the global ice volume~~, and it reconstructs either GMSL or $\delta^{18}O$ over the Quaternary. Internal feedback mechanisms and forcings are conceptualized by aggregated model parameters. This limits the physical ~~interpretation~~ interpretability of potential mechanisms driving the climate evolution. Hence, it would be beneficial to include other climatic variables in future work, e.g. CO_2. This would allow ~~to model~~ us to reconstruct the past evolution of ~~other climatic variables~~ them and improve the physical interpretability of the ~~results. Furthermore, it would make the models more robust since they would no longer depend on a single tuning target, which can lead to the reproduction of biases or errors, already present in the data~~modelled results. The early onset of the ramp-like change emphasizes the importance of intensifying the work to obtain an even older continuous ice core record than the recently drilled at least ~ 1.2 Ma old ice from the European Beyond EPICA-Oldest Ice Core project.

. The source code of the conceptual model and all the code and data to re-create the figures are publicly available on GitHub: https://github.com/felyx04/Conceptual-Model-Pollak-et-al-2025. The version corresponding to this submitted manuscript is available on Zenodo: https://doi.org/10.5281/zenodo.15421084.

. F.Po. and F.Pa. designed the conceptual model; F.Po. ran the simulations with the help of F.Pa.; Analysis performed by F.Po., with inputs from F.Pa., E.C., Z.C. and L.J.; F.Po. wrote a draft of the paper, with subsequent inputs from F.Pa., E.C., Z.C., L.J. and E.L.

. The authors declare that there are no competing interests.

. This study is an outcome of the AUFRANDE project, which is co-funded by the European Union under the Marie Skłodowska-Curie Grant Agreement No 101081465 (AUFRANDE). Views and opinions expressed are~~however~~ , however, those of the authors only and do not necessarily reflect those of the European Union or the Research Executive Agency. Neither the European Union nor the Research Executive Agency can be held responsible for them. This publication was also generated in the frame of Beyond EPICA. The project has received funding from the European Union's Horizon 2020 research and innovation programme under grant agreement No. 730258 (Oldest Ice) and No. 815384 (Oldest Ice Core). It is supported by national partners and funding agencies in Belgium, Denmark, France, Germany, Italy, Norway, Sweden, Switzerland, the Netherlands and the United Kingdom. Logistic support is mainly provided by ENEA and IPEV through the Concordia Station system. The opinions expressed and arguments employed herein do not necessarily reflect the official views of the European Union funding agency or other national funding bodies. This is Beyond EPICA publication number 45. E.C. received the financial

support from the French National Research Agency under the 'Programme d'Investissements d'Avenir' through the Make Our Planet Great Again HOTCLIM project (ANR-19-MPGA-0001). E.L. was supported by the Belgian Science Policy Office (BELSPO; FROID project).

References

Ahn, S., Khider, D., Lisiecki, L. E., and Lawrence, C. E.: A probabilistic Pliocene–Pleistocene stack of benthic δ18O using a profile hidden Markov model, Dynamics and Statistics of the Climate System, 2, dzx002, https://doi.org/10.1093/climsys/dzx002, 2017.

Austermann, J., Mitrovica, J. X., Latychev, K., and Milne, G. A.: Barbados-based estimate of ice volume at Last Glacial Maximum affected by subducted plate, Nature Geoscience, 6, 553–557, https://doi.org/10.1038/ngeo1859, publisher: Nature Publishing Group, 2013.

Barker, S. and Knorr, G.: A Systematic Role for Extreme Ocean-Atmosphere Oscillations in the Development of Glacial Conditions Since the Mid Pleistocene Transition, Paleoceanography and Paleoclimatology, 38, e2023PA004 690, https://doi.org/10.1029/2023PA004690, _eprint: https://onlinelibrary.wiley.com/doi/pdf/10.1029/2023PA004690, 2023.

Barker, S., Starr, A., van der Lubbe, J., Doughty, A., Knorr, G., Conn, S., Lordsmith, S., Owen, L., Nederbragt, A., Hemming, S., Hall, I., Levay, L., and IODP EXP 361 SHIPBOARD SCIENTIFIC PARTY: Persistent influence of precession on northern ice sheet variability since the early Pleistocene, Science, 376, 961–967, https://doi.org/10.1126/science.abm4033, publisher: American Association for the Advancement of Science, 2022.

Barker, S., Lisiecki, L. E., Knorr, G., Nuber, S., and Tzedakis, P. C.: Distinct roles for precession, obliquity, and eccentricity in Pleistocene 100-kyr glacial cycles, Science, 387, eadp3491, https://doi.org/10.1126/science.adp3491, publisher: American Association for the Advancement of Science, 2025.

Bereiter, B., Eggleston, S., Schmitt, J., Nehrbass-Ahles, C., Stocker, T. F., Fischer, H., Kipfstuhl, S., and Chappellaz, J.: Revision of the EPICA Dome C CO2 record from 800 to 600 kyr before present, Geophysical Research Letters, 42, 542–549, https://doi.org/10.1002/2014GL061957, _eprint: https://onlinelibrary.wiley.com/doi/pdf/10.1002/2014GL061957, 2015.

Berends, C. J., de Boer, B., and van de Wal, R. S. W.: Reconstructing the evolution of ice sheets, sea level, and atmospheric CO_2 during the past 3.6 million years, Climate of the Past, 17, 361–377, https://doi.org/10.5194/cp-17-361-2021, publisher: Copernicus GmbH, 2021a.

Berends, C. J., Köhler, P., Lourens, L. J., and van de Wal, R. S. W.: On the Cause of the Mid-Pleistocene Transition, Reviews of Geophysics, 59, e2020RG000 727, https://doi.org/10.1029/2020RG000727, _eprint: https://onlinelibrary.wiley.com/doi/pdf/10.1029/2020RG000727, 2021b.

Bintanja, R. and van de Wal, R. S. W.: North American ice-sheet dynamics and the onset of 100,000-year glacial cycles, Nature, 454, 869–872, https://doi.org/10.1038/nature07158, publisher: Nature Publishing Group, 2008.

Calder, N.: Arithmetic of ice ages, Nature, 252, 216–218, https://doi.org/10.1038/252216a0, publisher: Nature Publishing Group, 1974.

CenCO_2PIP Consortium: Toward a Cenozoic history of atmospheric CO2, Science, 382, eadi5177, https://doi.org/10.1126/science.adi5177, publisher: American Association for the Advancement of Science, 2023.

Chalk, T. B., Hain, M. P., Foster, G. L., Rohling, E. J., Sexton, P. F., Badger, M. P. S., Cherry, S. G., Hasenfratz, A. P., Haug, G. H., Jaccard, S. L., Martínez-García, A., Pälike, H., Pancost, R. D., and Wilson, P. A.: Causes of ice age intensification across the Mid-Pleistocene Transition, Proceedings of the National Academy of Sciences, 114, 13 114–13 119, https://doi.org/10.1073/pnas.1702143114, publisher: Proceedings of the National Academy of Sciences, 2017.

Clark, P. U. and Pollard, D.: Origin of the Middle Pleistocene Transition by ice sheet erosion of regolith, Paleoceanography, 13, 1–9, https://doi.org/10.1029/97PA02660, _eprint: https://onlinelibrary.wiley.com/doi/pdf/10.1029/97PA02660, 1998.

Clark, P. U., Archer, D., Pollard, D., Blum, J. D., Rial, J. A., Brovkin, V., Mix, A. C., Pisias, N. G., and Roy, M.: The middle Pleistocene transition: characteristics, mechanisms, and implications for long-term changes in atmospheric pCO2, Quaternary Science Reviews, 25, 3150–3184, https://doi.org/10.1016/j.quascirev.2006.07.008, 2006.

Clark, P. U., Shakun, J. D., Rosenthal, Y., Köhler, P., and Bartlein, P. J.: Global and regional temperature change over the past 4.5 million years, Science, 383, 884–890, https://doi.org/10.1126/science.adi1908, publisher: American Association for the Advancement of Science, 2024.

Clark, P. U., Shakun, J. D., Rosenthal, Y., Zhu, C., Bartlein, P. J., Gregory, J. M., Köhler, P., Liu, Z., and Schrag, D. P.: Mean ocean temperature change and decomposition of the benthic δ^{18}O record over the past 4.5 million years, Climate of the Past, 21, 973–1000, https://doi.org/10.5194/cp-21-973-2025, publisher: Copernicus GmbH, 2025.

Da, J., Zhang, Y. G., Li, G., Meng, X., and Ji, J.: Low CO2 levels of the entire Pleistocene epoch, Nature Communications, 10, 4342, https://doi.org/10.1038/s41467-019-12357-5, publisher: Nature Publishing Group, 2019.

Elderfield, H., Ferretti, P., Greaves, M., Crowhurst, S., McCave, I. N., Hodell, D., and Piotrowski, A. M.: Evolution of Ocean Temperature and Ice Volume Through the Mid-Pleistocene Climate Transition, Science, 337, 704–709, https://doi.org/10.1126/science.1221294, publisher: American Association for the Advancement of Science, 2012.

Farmer, J. R., Pico, T., Underwood, O. M., Cleveland Stout, R., Granger, J., Cronin, T. M., Fripiat, F., Martínez-García, A., Haug, G. H., and Sigman, D. M.: The Bering Strait was flooded 10,000 years before the Last Glacial Maximum, Proceedings of the National Academy of Sciences, 120, e2206742 119, https://doi.org/10.1073/pnas.2206742119, publisher: Proceedings of the National Academy of Sciences, 2023.

Foreman-Mackey, D., Hogg, D. W., Lang, D., and Goodman, J.: emcee: The MCMC Hammer, Publications of the Astronomical Society of the Pacific, 125, 306–312, https://doi.org/10.1086/670067, arXiv:1202.3665 [astro-ph, physics:physics, stat], 2013.

Ganopolski, A.: Toward generalized Milankovitch theory (GMT), Climate of the Past, 20, 151–185, https://doi.org/10.5194/cp-20-151-2024, publisher: Copernicus GmbH, 2024.

Ganopolski, A., Winkelmann, R., and Schellnhuber, H. J.: Critical insolation–CO2 relation for diagnosing past and future glacial inception, Nature, 529, 200–203, https://doi.org/10.1038/nature16494, publisher: Nature Publishing Group, 2016.

Gildor, H. and Tziperman, E.: A sea ice climate switch mechanism for the 100-kyr glacial cycles, Journal of Geophysical Research: Oceans, 106, 9117–9133, https://doi.org/10.1029/1999JC000120, _eprint: https://onlinelibrary.wiley.com/doi/pdf/10.1029/1999JC000120, 2001.

Goodman, J. and Weare, J.: Ensemble samplers with affine invariance, Communications in Applied Mathematics and Computational Science, 5, 65–80, https://doi.org/10.2140/camcos.2010.5.65, publisher: Mathematical Sciences Publishers, 2010.

Gregoire, L. J., Payne, A. J., and Valdes, P. J.: Deglacial rapid sea level rises caused by ice-sheet saddle collapses, Nature, 487, 219–222, https://doi.org/10.1038/nature11257, publisher: Nature Publishing Group, 2012.

Hays, J. D., Imbrie, J., and Shackleton, N. J.: Variations in the Earth's Orbit: Pacemaker of the Ice Ages, Science, 194, 1121–1132, https://www.jstor.org/stable/1743620, publisher: American Association for the Advancement of Science, 1976.

Huybers, P.: Early Pleistocene Glacial Cycles and the Integrated Summer Insolation Forcing, Science, 313, 508–511, https://doi.org/10.1126/science.1125249, publisher: American Association for the Advancement of Science, 2006.

Hönisch, B., Hemming, N. G., Archer, D., Siddall, M., and McManus, J. F.: Atmospheric Carbon Dioxide Concentration across the Mid-Pleistocene Transition, Science, 324, 1551–1554, https://www.jstor.org/stable/20494191, publisher: American Association for the Advancement of Science, 2009.

Imbrie, J. and Imbrie, J. Z.: Modeling the Climatic Response to Orbital Variations, Science, 207, 943–953, https://doi.org/10.1126/science.207.4434.943, publisher: American Association for the Advancement of Science, 1980.

Imbrie, J. Z., Imbrie-Moore, A., and Lisiecki, L. E.: A phase-space model for Pleistocene ice volume, Earth and Planetary Science Letters, 307, 94–102, https://doi.org/10.1016/j.epsl.2011.04.018, arXiv:1104.3610 [astro-ph, physics:physics], 2011.

Koposov, S., Speagle, J., Barbary, K., Ashton, G., Bennett, E., Buchner, J., Scheffler, C., Cook, B., Talbot, C., Guillochon, J., Cubillos, P., Ramos, A. A., Dartiailh, M., Ilya, Tollerud, E., Lang, D., Johnson, B., jtmendel, Higson, E., Vandal, T., Daylan, T., Angus, R., patelR, Cargile, P., Sheehan, P., Pitkin, M., Kirk, M., Leja, J., joezuntz, and Goldstein, D.: joshspeagle/dynesty: v2.1.4, https://doi.org/10.5281/zenodo.12537467, 2024.

Köhler, P. and van de Wal, R. S. W.: Interglacials of the Quaternary defined by northern hemispheric land ice distribution outside of Greenland, Nature Communications, 11, 5124, https://doi.org/10.1038/s41467-020-18897-5, publisher: Nature Publishing Group, 2020.

Lambeck, K., Rouby, H., Purcell, A., Sun, Y., and Sambridge, M.: Sea level and global ice volumes from the Last Glacial Maximum to the Holocene, Proceedings of the National Academy of Sciences, 111, 15 296–15 303, https://doi.org/10.1073/pnas.1411762111, publisher: Proceedings of the National Academy of Sciences, 2014.

Laskar, J., Robutel, P., Joutel, F., Gastineau, M., Correia, A. C. M., and Levrard, B.: A long-term numerical solution for the insolation quantities of the Earth, Astronomy & Astrophysics, 428, 261–285, https://doi.org/10.1051/0004-6361:20041335, publisher: EDP Sciences, 2004.

Legrain, E.: Interactions between the climate and the carbon cycle at centennial-to-orbital timescales over the past 2 million years, Ph.D. thesis, University Grenoble, Grenoble, 2023.

Legrain, E., Parrenin, F., and Capron, E.: A gradual change is more likely to have caused the Mid-Pleistocene Transition than an abrupt event, Communications Earth & Environment, 4, 1–10, https://doi.org/10.1038/s43247-023-00754-0, number: 1 Publisher: Nature Publishing Group, 2023.

Leloup, G. and Paillard, D.: Influence of the choice of insolation forcing on the results of a conceptual glacial cycle model, Climate of the Past, 18, 547–558, https://doi.org/10.5194/cp-18-547-2022, publisher: Copernicus GmbH, 2022.

Lisiecki, L. E.: Atlantic overturning responses to obliquity and precession over the last 3 Myr, Paleoceanography, 29, 71–86, https://doi.org/10.1002/2013PA002505, _eprint: https://agupubs.onlinelibrary.wiley.com/doi/pdf/10.1002/2013PA002505, 2014.

Lisiecki, L. E. and Raymo, M. E.: A Pliocene-Pleistocene stack of 57 globally distributed benthic δ18O records, Paleoceanography, 20, https://doi.org/10.1029/2004PA001071, _eprint: https://onlinelibrary.wiley.com/doi/pdf/10.1029/2004PA001071, 2005.

Loutre, M.-F.: Paramètres orbitaux et cycles diurne et saisonnier des insolations, Ph.D. thesis, UCL - Université Catholique de Louvain, https://dial.uclouvain.be/pr/boreal/object/boreal:205325, 1993.

Ma, X., Yang, M., Sun, Y., Dang, H., Ma, W., Tian, J., Jiang, Q., Liu, L., Jin, X., and Jin, Z.: The potential role of insolation in the long-term climate evolution since the early Pleistocene, Global and Planetary Change, 240, 104 526, https://doi.org/10.1016/j.gloplacha.2024.104526, 2024.

McClymont, E. L., Sosdian, S. M., Rosell-Melé, A., and Rosenthal, Y.: Pleistocene sea-surface temperature evolution: Early cooling, delayed glacial intensification, and implications for the mid-Pleistocene climate transition, Earth-Science Reviews, 123, 173–193, https://doi.org/10.1016/j.earscirev.2013.04.006, 2013.

Milankovitch, M.: Kanon der Erdbestrahlung und seine Anwendung auf das Eiszeitenproblem, Royal Serbian Academy Special Publication, 133, 1–633, https://cir.nii.ac.jp/crid/1572824499597240704, publisher: Israel Program for Sceientific Translation, U. S. Department of Commerce, 1941.

Mitsui, T. and Crucifix, M.: Influence of external forcings on abrupt millennial-scale climate changes: a statistical modelling study, Climate Dynamics, 48, 2729–2749, https://doi.org/10.1007/s00382-016-3235-z, 2017.

Mitsui, T., Tzedakis, P. C., and Wolff, E. W.: Insolation evolution and ice volume legacies determine interglacial and glacial intensity, Climate of the Past, 18, 1983–1996, https://doi.org/10.5194/cp-18-1983-2022, publisher: Copernicus GmbH, 2022.

Nyman, K. H. M. and Ditlevsen, P. D.: The middle Pleistocene transition by frequency locking and slow ramping of internal period, Climate Dynamics, 53, 3023–3038, https://doi.org/10.1007/s00382-019-04679-3, company: Springer Distributor: Springer Institution: Springer Label: Springer Number: 5 Publisher: Springer Berlin Heidelberg, 2019.

Paillard, D.: The timing of Pleistocene glaciations from a simple multiple-state climate model, Nature, 391, 378–381, https://doi.org/10.1038/34891, publisher: Nature Publishing Group, 1998.

Paillard, D.: Quaternary glaciations: from observations to theories, Quaternary Science Reviews, 107, 11–24, https://doi.org/10.1016/j.quascirev.2014.10.002, 2015.

Paillard, D. and Parrenin, F.: The Antarctic ice sheet and the triggering of deglaciations, Earth and Planetary Science Letters, 227, 263–271, https://doi.org/10.1016/j.epsl.2004.08.023, 2004.

Parrenin, F. and Paillard, D.: Amplitude and phase of glacial cycles from a conceptual model, Earth and Planetary Science Letters, 214, 243–250, https://doi.org/10.1016/S0012-821X(03)00363-7, 2003.

Parrenin, F. and Paillard, D.: Terminations VI and VIII ($\sim$ 530 and $\sim$ 720 kyr BP) tell us the importance of obliquity and precession in the triggering of deglaciations, Climate of the Past, 8, 2031–2037, https://doi.org/10.5194/cp-8-2031-2012, 2012.

Peterson, J. M., Shackleton, S., Higgins, J., Severinghaus, J., Yan, Y., Buizert, C., Kalk, M., Beaudette, R., Hishamunda, V., Carter, A., Kurbatov, A., Epifanio, J., Morgan, J., Bender, M., and Brook, E.: Ice cores from the Allan Hills, Antarctica show relatively stable atmospheric CO2 and CH4 levels over the last 3 million years, https://doi.org/10.21203/rs.3.rs-5610566/v1, iSSN: 2693-5015, 2024.

Pérez-Montero, S., Alvarez-Solas, J., Swierczek-Jereczek, J., Moreno-Parada, D., Montoya, M., and Robinson, A.: A simple physical model for glacial cycles, EGUsphere, pp. 1–29, https://doi.org/10.5194/egusphere-2024-1842, publisher: Copernicus GmbH, 2024.

Raftery, A. E.: Bayesian Model Selection in Social Research, Sociological Methodology, 25, 111–163, https://doi.org/10.2307/271063, publisher: [American Sociological Association, Wiley, Sage Publications, Inc.], 1995.

Raymo, M. E. and Huybers, P.: Unlocking the mysteries of the ice ages, Nature, 451, 284–285, https://doi.org/10.1038/nature06589, number: 7176 Publisher: Nature Publishing Group, 2008.

Rohling, E. J., Yu, J., Heslop, D., Foster, G. L., Opdyke, B., and Roberts, A. P.: Sea level and deep-sea temperature reconstructions suggest quasi-stable states and critical transitions over the past 40 million years, Science Advances, 7, eabf5326, https://doi.org/10.1126/sciadv.abf5326, publisher: American Association for the Advancement of Science, 2021.

Rohling, E. J., Foster, G. L., Gernon, T. M., Grant, K. M., Heslop, D., Hibbert, F. D., Roberts, A. P., and Yu, J.: Comparison and Synthesis of Sea-Level and Deep-Sea Temperature Variations Over the Past 40 Million Years, Reviews of Geophysics, 60, e2022RG000 775, https://doi.org/10.1029/2022RG000775, _eprint: https://onlinelibrary.wiley.com/doi/pdf/10.1029/2022RG000775, 2022.

Saltzman, B.: Dynamical Paleoclimatology: Generalized Theory of Global Climate Change, Elsevier, ISBN 978-0-08-050483-4, google-Books-ID: Y975LsF3Q_wC, 2001.

Scherrenberg, M. D. W., Berends, C. J., and van de Wal, R. S. W.: CO_2 and summer insolation as drivers for the Mid-Pleistocene Transition, Climate of the Past, 21, 1061–1077, https://doi.org/10.5194/cp-21-1061-2025, publisher: Copernicus GmbH, 2025.

Speagle, J. S.: DYNESTY: a dynamic nested sampling package for estimating Bayesian posteriors and evidences, Monthly Notices of the Royal Astronomical Society, 493, 3132–3158, https://doi.org/10.1093/mnras/staa278, publisher: OUP ADS Bibcode: 2020MNRAS.493.3132S, 2020.

Talento, S. and Ganopolski, A.: Reduced-complexity model for the impact of anthropogenic CO_2 emissions on future glacial cycles, Earth System Dynamics, 12, 1275–1293, https://doi.org/10.5194/esd-12-1275-2021, publisher: Copernicus GmbH, 2021.

Ter Braak, C. J. F. and Vrugt, J. A.: Differential Evolution Markov Chain with snooker updater and fewer chains, Statistics and Computing, 18, 435–446, https://doi.org/10.1007/s11222-008-9104-9, 2008.

Tzedakis, P. C., Crucifix, M., Mitsui, T., and Wolff, E. W.: A simple rule to determine which insolation cycles lead to interglacials, Nature, 542, 427–432, https://doi.org/10.1038/nature21364, publisher: Nature Publishing Group, 2017.

Verbitsky, M. and Omta, A. W.: Rapid Communication: Middle Pleistocene Transition as a Phenomenon of Orbitally Enabled Sensitivity to Initial Values, EGUsphere, pp. 1–9, https://doi.org/10.5194/egusphere-2025-3334, publisher: Copernicus GmbH, 2025.

Verbitsky, M. Y. and Crucifix, M.: Do phenomenological dynamical paleoclimate models have physical similarity with Nature? Seemingly, not all of them do, Climate of the Past, 19, 1793–1803, https://doi.org/10.5194/cp-19-1793-2023, publisher: Copernicus GmbH, 2023.

Vousden, W., Farr, W. M., and Mandel, I.: Dynamic temperature selection for parallel-tempering in Markov chain Monte Carlo simulations, Monthly Notices of the Royal Astronomical Society, 455, 1919–1937, https://doi.org/10.1093/mnras/stv2422, arXiv:1501.05823 [astro-ph], 2016.

Weber, M. E., Bailey, I., Hemming, S. R., Martos, Y. M., Reilly, B. T., Ronge, T. A., Brachfeld, S., Williams, T., Raymo, M., Belt, S. T., Smik, L., Vogel, H., Peck, V. L., Armbrecht, L., Cage, A., Cardillo, F. G., Du, Z., Fauth, G., Fogwill, C. J., Garcia, M., Garnsworthy, M., Glüder, A., Guitard, M., Gutjahr, M., Hernández-Almeida, I., Hoem, F. S., Hwang, J.-H., Iizuka, M., Kato, Y., Kenlee, B., OConnell, S., Pérez, L. F., Seki, O., Stevens, L., Tauxe, L., Tripathi, S., Warnock, J., and Zheng, X.: Antiphased dust deposition and productivity in the Antarctic Zone over 1.5 million years, Nature Communications, 13, 2044, https://doi.org/10.1038/s41467-022-29642-5, number: 1 Publisher: Nature Publishing Group, 2022.

Willeit, M., Ganopolski, A., Calov, R., and Brovkin, V.: Mid-Pleistocene transition in glacial cycles explained by declining CO2 and regolith removal, Science Advances, 5, eaav7337, https://doi.org/10.1126/sciadv.aav7337, publisher: American Association for the Advancement of Science, 2019.

Yamamoto, M., Clemens, S. C., Seki, O., Tsuchiya, Y., Huang, Y., O'ishi, R., and Abe-Ouchi, A.: Increased interglacial atmospheric CO2 levels followed the mid-Pleistocene Transition, Nature Geoscience, 15, 307–313, https://doi.org/10.1038/s41561-022-00918-1, publisher: Nature Publishing Group, 2022.

Yan, Y., Bender, M. L., Brook, E. J., Clifford, H. M., Kemeny, P. C., Kurbatov, A. V., Mackay, S., Mayewski, P. A., Ng, J., Severinghaus, J. P., and Higgins, J. A.: Two-million-year-old snapshots of atmospheric gases from Antarctic ice, Nature, 574, 663–666, https://doi.org/10.1038/s41586-019-1692-3, number: 7780 Publisher: Nature Publishing Group, 2019.

Yehudai, M., Kim, J., Pena, L. D., Jaume-Seguí, M., Knudson, K. P., Bolge, L., Malinverno, A., Bickert, T., and Goldstein, S. L.: Evidence for a Northern Hemispheric trigger of the 100,000-y glacial cyclicity, Proceedings of the National Academy of Sciences, 118, e2020260 118, https://doi.org/10.1073/pnas.2020260118, publisher: Proceedings of the National Academy of Sciences, 2021.

Yokoyama, Y., Lambeck, K., De Deckker, P., Johnston, P., and Fifield, L. K.: Timing of the Last Glacial Maximum from observed sea-level minima, Nature, 406, 713–716, https://doi.org/10.1038/35021035, publisher: Nature Publishing Group, 2000.

~~Tuned parameter values for the best 2.6 Myr simulation runs of the five different models used in this study. The values are rounded to four decimal places. $\text{state}_{\text{initial}}$ sets the initial state in which the model starts the simulation. This parameter was not used as a tunable parameter, but instead always set to glacial mode.~~ **Parameter ORB ABR GRAD RAMP RAMP-I** ~~α_{Esi} () 0.6079, 0.0545 -0.2797 0.0924 0.3835 α_{Eco} () -0.5484 -0.2323 -0.4106 -0.1446 -0.2152 α_{O} () 1.2801 0.8058 0.7678 0.5871 0.7968 α_{g} () 0.3237 0.8641 0.9035 0.8900 0.9908 α_{d} () -0.2705 -0.8056 0.1736 0.1647 -0.4266 τ_d () 1954.8438 7.0156 5.2301 6.3376 5.3454 k_{Esi} () 583.8280 18.8947 21.8939 17.6969 -10.7672 k_{Eco} () 9198.7910 3.7642 7.7095 1.4041 -6.1782 k_{O} ()~~

567.0562 6.3133 12.4559 11.5707 0.8189 v_0 () -4598.8362 96.7743 126.3573 98.3877 127.3623 v_1 () 4919.8064 -1.7411 -10.4710 2.3544 -0.8391 v_i () 19.8410 17.9954 9.2756 9.1767 17.9847 $\text{state}_{\text{initial}}$ glacial glacial glacial glacial glacial t_{abr} () / 1246.0466 / / / v_0' () / 10.5984 / -12.9160 20.6520 τ_d' () / -113.2884 / 31.4175 41.1961 C_v () / / 0.0409 / / C_τ () / / -0.0056 / / t_2 () / / / 2159.3461 1977.8274 t_1 () / / / 857.9326 454.2691 l_{Esi} (unitless) / / / / 0.6750 l_{Eco} (unitless) / / / / 0.1366 l_{O} (unitless) / / / / 0.1446 # Parameters 12 15 14 16 19 (excluding $\text{state}_{\text{initial}}$)

Root mean square errors (RMSEs) and coefficient of determination (R^2) for the five different model configurations for various time periods. **Period (Ma)Model RMSE** R^2 **RMSE** R^2 **RMSE** R^2 **RMSE** R^2 ORB 10.58 0.49 17.12 0.20 25.56 0.18 17.50 0.47 ABR 10.60 0.49 13.90 0.47 13.92 0.76 12.24 0.74 GRAD 10.06 0.54 13.18 0.52 13.87 0.76 11.86 0.76 RAMP 10.01 0.54 11.73 0.62 13.30 0.78 11.38 0.78 RAMP-I 8.14 0.70 13.09 0.53 11.16 0.84 10.02 0.83

Residuals of the four different model configurations wrt the ice-volume reconstruction by Berends et al. (2021a). The residuals are calculated as *model-data*. The residuals are shown for the ORB (**a**, black curve), ABR (**b**, red curve), GRAD (**c**, green curve) and the RAMP model (**d**, purple curve) over the whole Pleistocene. The blue-shaded area marks where the simulation exceeds a residual of -20 , while the red-shaded area marks where the simulation exceeds a residual of $+20$.

Comparison of the four different model configurations. The simulated ice volume curves are shown for the ORB (**a**, black curve), ABR (**b**, red curve), GRAD (**c**, green curve) and the RAMP model (**d**, purple curve) over the last 2 Ma. Each simulation is plotted over the ice volume reconstruction by Berends et al. (2021a) (blue curve). The deglaciation parameter $v_0(t)$ (black dotted line) is shown for each simulation, indicating the internal forcing scenario. The yellow shaded area marks the future 250 kyr and the respective predictions by each model. The grey-shaded area highlights the classical perspective of where the MPT is located in time. MIS boundaries given according to Lisiecki and Raymo (2005).

Comparison of the four different model configurations. The simulated ice volume curves are shown for the ORB (**a**, black curve), ABR (**b**, red curve), GRAD (**c**, green curve) and the RAMP model (**d**, purple curve) over the last 3.6 Ma. Each simulation is plotted over the ice volume reconstruction by Berends et al. (2021a) (blue curve). The deglaciation parameter $v_0(t)$ (black dotted line) is shown for each simulation, indicating the internal forcing scenario. The yellow shaded area marks the future 250 kyr and the respective predictions by each model. The grey-shaded area highlights the classical perspective of where the MPT is located in time. MIS boundaries given according to Lisiecki and Raymo (2005).

(Same Figure as Figure **??**, but models are based on a different ice volume reconstruction) Comparison of the four different model configurations. The simulated ice volume curves are shown for the ORB (**a**, black curve), ABR (**b**, red curve), GRAD (**c**, green curve) and the RAMP model (**d**, purple curve) over the whole Pleistocene. Each simulation is plotted over the ice volume reconstruction by Rohling et al. (2022) (blue curve). The deglaciation parameter $v_0(t)$ (black dotted line) is shown for each simulation, indicating the internal forcing scenario. The yellow shaded area marks the future 250 kyr and the respective predictions by each model. The grey-shaded area highlights the classical perspective of where the MPT is located in time. MIS boundaries given according to Lisiecki and Raymo (2005).

Comparison of the four model configurations, tuned for different targets, over the whole Pleistocene. Each panel shows one of the four model configurations (ORB, ABR, GRAD and RAMP model), once tuned for the Berends sea-level reconstruction (coloured dashed lines) and once tuned for the Rohling sea-level reconstruction (coloured solid lines). The corresponding

deglaciation parameter $v_0(t)$ is shown for each model, indicating the internal forcing scenario (Berends-based model: grey dashed line, Rohling-based model: grey solid line). The yellow shaded area marks the future 250 kyr and the respective predictions by each model. The grey-shaded area highlights the classical perspective of where the MPT is located in time.

Simulated ice volume by the RAMP-1 model (golden line) for period 1.2 – 0.6 Ma, together with its deglaciation and glaciation thresholds. The forcing $\tilde{I}_\kappa(t)$ is shown in red. While the red shaded area marks forcing values above the model threshold v_1, the blue shaded area marks values below. The time-dependent deglaciation parameter $v_0(t)$ is represented by the black dotted line, while the solid black line indicates the deglaciation threshold. The purple dots indicate terminations, and the red dots mark glacial inceptions.